Allahdadi et al OSM2018

Presentation · February 2018

DOI: 10.13140/RG.2.2.22754.43207

5 authors, including:

Nabi Allahdadi
North Carolina State University
33 PUBLICATIONS **48** CITATIONS

SEE PROFILE

Budi Gunawan
Sandia National Laboratories
46 PUBLICATIONS **252** CITATIONS

SEE PROFILE

2018 OCEAN SCIENCES MEETING

AGU • ASLO • The Oceanography Society

11–16 February • Portland, Oregon, USA

High Resolution Wave modeling for Characterizing Wave Energy Resources along the U.S East Coast

Nabi Allahdadi[1], Budi Gunawan[2], Jonathan Lai[2], Ruoying He[1], Vincent S. Neary[2]

1. North Carolina State University
2. Sandia National Laboratories

NC STATE UNIVERSITY

OOMG
OCEAN OBSERVING AND MODELING GROUP

Sandia National Laboratories

Motivation

- The global need to diversify energy portfolios, expand energy supplies and reduce carbon emissions
- Renewable energy supplied by ocean waves and swells can be converted to electricity using an assortment of technologies known as wave energy converters (WEC)
- The potential wave energy resource for the United States is about ten-percent of the global resource
- Resource characterization and assessment is an important first step to develop this wave energy resource potential and it supports a broad range of regional planning, project development and WEC design activities

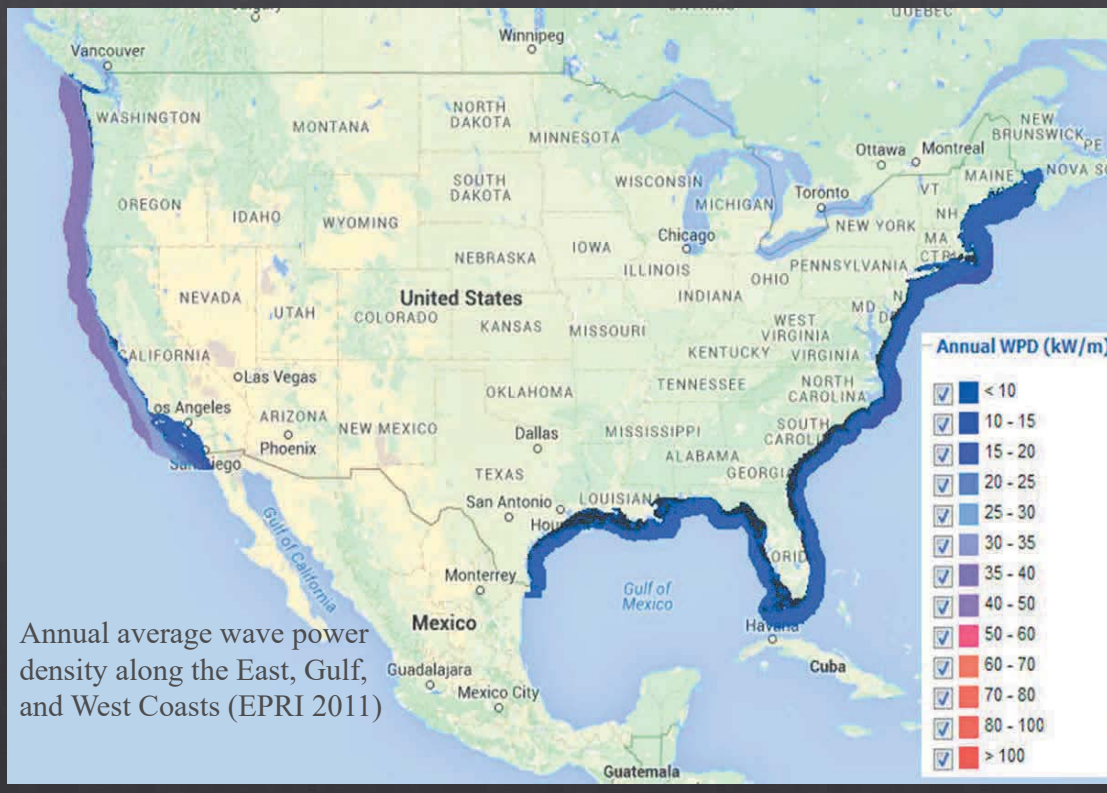

Annual average wave power density along the East, Gulf, and West Coasts (EPRI 2011)

Objectives

- Preparing a long-term modeling database for waves along the East Coast based on a high spatial resolution computational mesh that is sufficient for high accuracy wave resource characterization

- Thorough calibration and verification of the model based on the 6 IEC parameters calculated at the location of coastal and offshore buoys and consistent with the test bed study along the Oregon Coast

- Presenting desired quantities including 6 IEC parameters and partitioned spectra at different locations and along the shoreline

Buoy data

- 18 NDBC buoys
- Both coastal and offshore
- All measured wave parameters including H_s, T_p, and T_{02}
- Only 7 of them measure directional spectra

Buoy	Depth(m)	Description	Longitude	Latitude
41002	3980	SOUTH HATTERAS - 225 NM South of Cape Hatteras	-74.840	31.76
41004	38.4	EDISTO - 41 NM Southeast of Charleston, SC	-79.099	32.501
41008	18.288	GRAYS REEF - 40 NM Southeast of Savannah, GA	-80.868	31.4
41010	888	CANAVERAL EAST - 120NM East of Cape Canaveral	-78.45	28.884
41013	23.5	Frying Pan Shoals, NC	-77.743	33.436
41025	68.3	Diamond Shoals, NC	-75.402	35.006
41047	5283	NE BAHAMAS - 350 NM ENE of Nassau, Bahamas	-71.479	27.485
41048	5340	WEST BERMUDA - 240 NM West of Bermuda	-69.590	31.86
44005	180.7	GULF OF MAINE - 78 NM East of Portsmouth, NH	-69.128	43.201
44007	26.5	PORTLAND 12 NM Southeast of Portland, ME	-70.141	43.525
44008	74.7	NANTUCKET 54NM Southeast of Nantucket	-69.248	40.504
44009	43	DELAWARE BAY 26 NM Southeast of Cape May, NJ	-74.703	38.461
44011	82.9	GEORGES BANK 170 NM East of Hyannis, MA	-66.619	41.098
44013	64.5	BOSTON 16 NM East of Boston, MA	-70.651	42.346
44017	52.4	MONTAUK POINT - 23 NM SSW of Montauk Point, NY	-72.048	40.694
44018	217.3	CAPE COD - 24 NM East of Provincetown, MA	-69.7	42.119
44025	40.8	LONG ISLAND - 30 NM South of Islip, NY	-73.164	40.251
44027	178.6	Jonesport, ME - 20 NM SE of Jonesport, ME	-67.307	44.287

Computational mesh

- Unstructured SWAN
- coastal resolution (within 20 km distance from the shoreline) : 200 meters
- Resolution along the offshore boundaries 10-15 km
- over 4,300,000 grid points

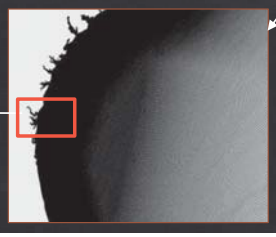

Map of spatial resolution

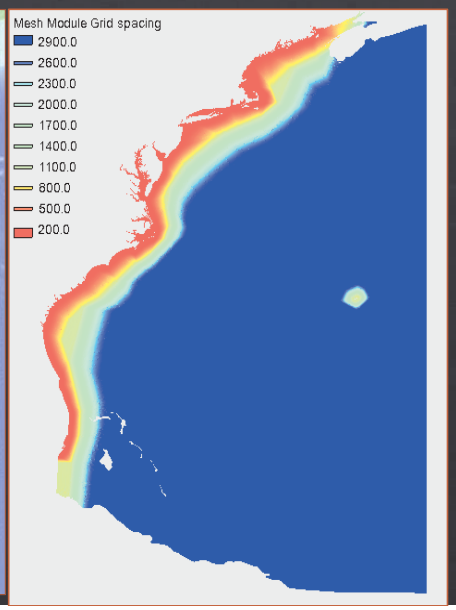

Wind Field

- Climate Forecast System Reanalysis (CFSR)
- Spatial resolution: 0.312 °
- Temporal resolution: 1 hour
- Seasonality

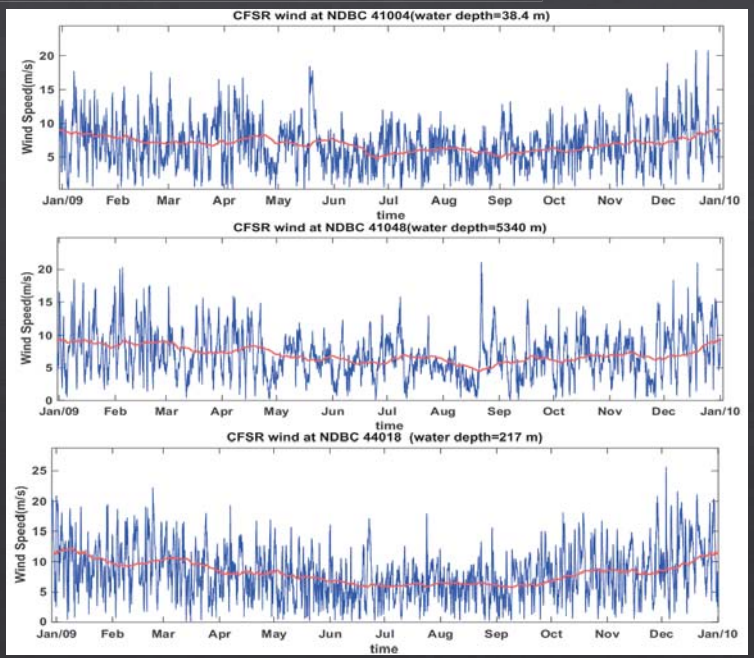

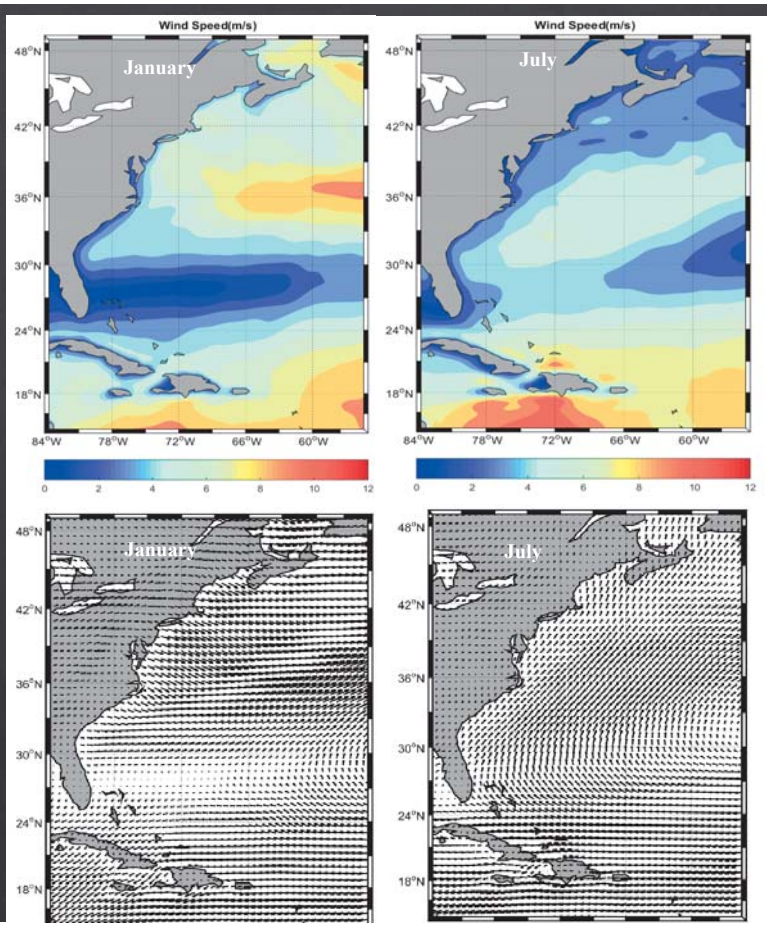

Boundary Conditions

- Global WWIII model implemented by NOAA (http://polar.ncep.noaa.gov/waves/hindcasts/nopp-phase2.php)
- Spatial resolution: 0.5 °
- Temporal resolution: 3 hours
- Physics package : ST4
- Wave parameters including height, peak period, and direction were prescribed along open boundaries

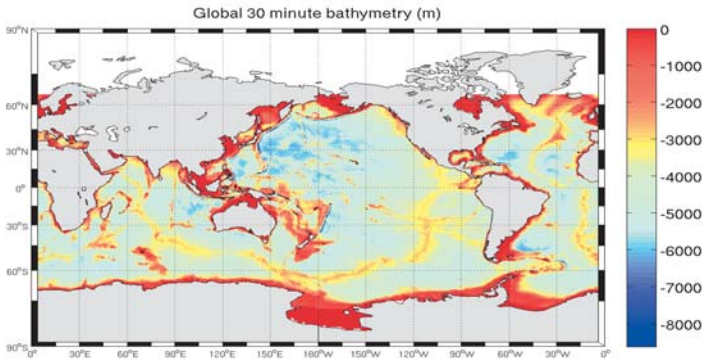

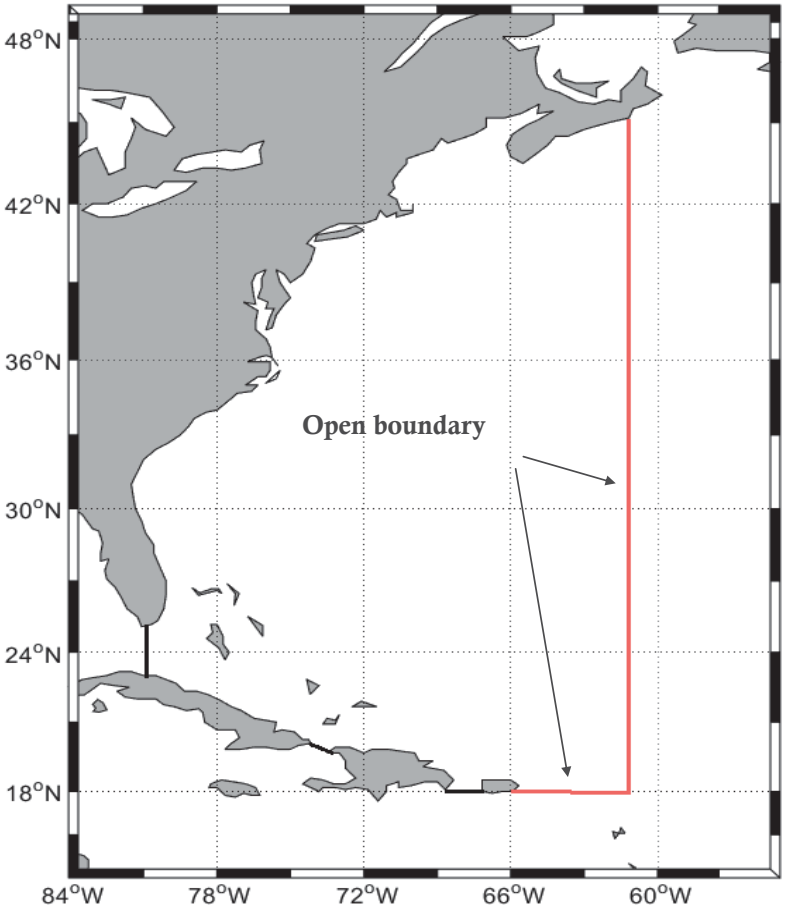

Model run

- 4,396,138 grid points
- 496 cores on the Sandia SkyBridge cluster~ 8700 node for each core
- Each month of simulation took about 6 hours

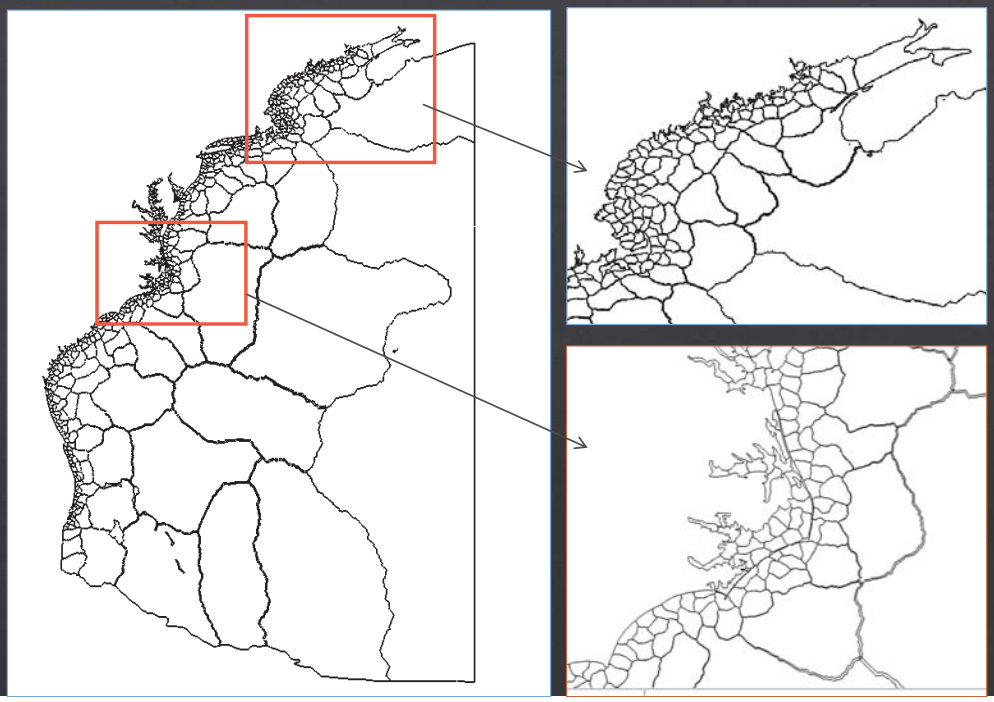

Model Sensitivity analysis

- Several model parameters are site or scale specific
- Regional wind and wave climate may be important

Parameter	Symbol	Examined values/Method	Selected value/Method
Computational time step	Δt	3, 5, 10, 20, 30, 50 minutes	10 min
Number of iterations	Nit	1, 3, 5, 7, 10	1
Directional standard deviation	DSD	20, 30, 50, 70	30 degrees
Frequency spectral shape		JONSWAP: $\gamma = 1.1, 3.3, 6, 7$ Pierson-Moskowitz	3.3
Number of spectral frequencies	Nf	18, 24, 28, 32	28
Number of spectral directions	Nd	18, 25, 36, 48	25

Model Calibration

Whitecapping dissipation and the associated parameters were used

Komen-type approaches (mean spectral parameters)
Komen(1984) and Janssen(1991)

$$S_{ds,w}(\sigma,\theta) = -\Gamma\tilde{\sigma}\,\frac{k}{\tilde{k}}E(\sigma,\theta)$$

$$\Gamma = C_{ds}\left((1-\delta)+\delta\frac{k}{\tilde{k}}\right)\left(\frac{\tilde{S}}{\tilde{S}_{PM}}\right)^{p}$$

$$\tilde{S}_{PM} = (3.02\times10^{-3})^{1/2}$$

$$\tilde{S} = \tilde{k}\sqrt{E_{tot}}$$

Saturated-based approach
Van der Westhuysen(2007)

$$S_{ds,break}(\sigma,\theta) = -C_{ds}\left[\frac{B(k)}{B_r}\right]^{p/2}[\tanh(kd)]^{\frac{2-p_0}{4}}\,g^{\frac{1}{2}}\,k^{\frac{1}{2}}E(\sigma,\theta)$$

$$S_{ds,w}(\sigma,\theta) = f_{br}(\sigma)S_{ds,break} + [1-f_{br}(\sigma)]S_{ds,non-break}$$

$S_{ds,non-break}$

accounts for dissipation by turbulence and short-wave-long-wave interaction

Three 1-month time periods were used for model calibration / measured waves at 18 NDBC buoys
different whitecapping formulations and different sets of parameters were examined

Janssen(1991) C_{ds}=2.7 δ=0.9

Model verification

Model performance metrics

$$R = \frac{\sum_{i=1}^{N}(M_i - \bar{M})(P_i - \bar{P})}{\sqrt{(\sum_{i=1}^{N}(M_i - \bar{M})^2)(\sum_{i=1}^{N}(P_i - \bar{P})^2)}}$$

$$bias(P) = \frac{\sum_{i=1}^{N}(P_i - M_i)}{N}$$

$$RMSE = \sqrt{\frac{\sum_{i=1}^{N}(P_i - M_i)^2}{N}}$$

$$SI = \frac{RMSE}{\bar{M}}$$

M: measurement P: model prediction

IEC parameters

Significant wave height	H_s
Energy period	T_e
Omnidirectiona wave power	$J = \rho g \sum_{i,j} c_{g,i}\ S_{ij} \Delta f_i \Delta \theta_j$ $[\frac{kW}{m}]$
Spectral width	$\epsilon_0 = \sqrt{\frac{m_0 m_{-2}}{m_{-1}^2} - 1}$
Direction of max power	θ_{Jmax}
Directionally coefficient	$d = \frac{J_{\theta_{Jmax}}}{J}$

i,j : number of spectral frequencies and directions, respectively

m : spectral moments

3-year verification from 2007 to 2009

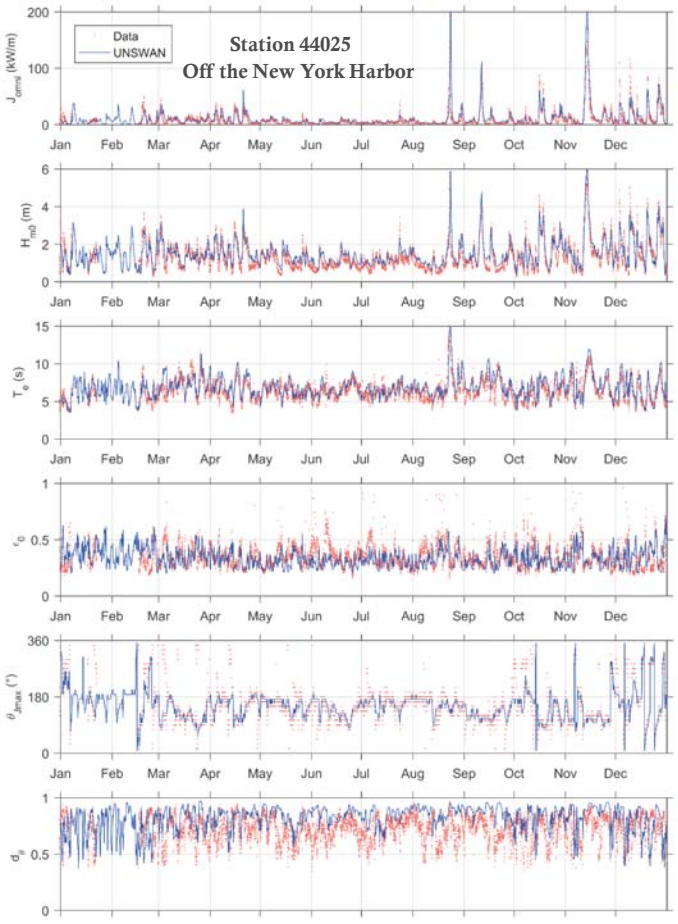
Data
UNSWAN
Station 44025
Off the New York Harbor
J_{omni} (kW/m)
H_{m0} (m)
T_e (s)
ϵ_0
θ_{Jmax} (°)
d_θ
Jan Feb Mar Apr May Jun Jul Aug Sep Oct Nov Dec

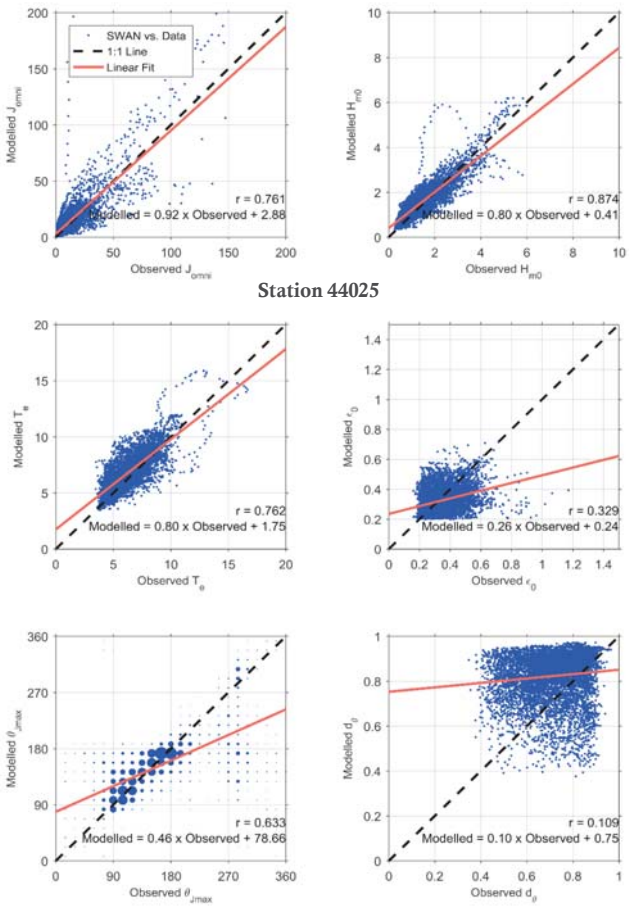
SWAN vs. Data
1:1 Line
Linear Fit
r = 0.761
Modelled = 0.92 x Observed + 2.88
Modelled J_{omni}
Observed J_{omni}
r = 0.874
Modelled = 0.80 x Observed + 0.41
Modelled H_{m0}
Observed H_{m0}
Station 44025
r = 0.762
Modelled = 0.80 x Observed + 1.75
Modelled T_e
Observed T_e
r = 0.329
Modelled = 0.26 x Observed + 0.24
Modelled ϵ_0
Observed ϵ_0
r = 0.633
Modelled = 0.46 x Observed + 78.66
Modelled θ_{Jmax}
Observed θ_{Jmax}
r = 0.109
Modelled = 0.10 x Observed + 0.75
Modelled d_θ
Observed d_θ

Model performance metrics at selected stations

Buoy	Parameter	RMSE	SI	Bias	R
41013					
	Hs(m)	0.31	0.24	0.13	0.91
	Te(s)	0.92	0.15	0.45	0.79
	ϵ_0(-)	6.44	0.82	2.12	0.90
	J(kw/m)	0.07	0.20	-0.01	0.59
	$\theta_{Jmax(degrees)}$	39.50	N/A	2.77	0.68
	d_θ (-)	0.14	0.19	0.07	0.37
41048	Hs(m)	0.38	0.20	0.14	0.93
	Te(s)	0.78	0.11	0.35	0.87
	ϵ_0(-)	14.94	0.85	3.53	0.88
	J(kw/m)	0.05	0.17	-0.02	0.65
	θ_{Jmax}(degrees)	39.63	N/A	0.92	0.70
	d_θ (-)	0.09	0.13	0.02	0.77
44018	Hs(m)	0.46	0.31	0.01	0.86
	Te(s)	1.13	0.17	-0.32	0.68
	ϵ_0(-)	11.07	0.98	-1.10	0.80
	J(kw/m)	0.09	0.27	0.03	0.45
	$\theta_{Jmax(degrees)}$	47.57	N/A	-3.20	0.55
	d_θ (-)	0.17	0.25	0.10	0.27
44025	Hs(m)	0.40	0.30	0.15	0.87
	Te(s)	1.12	0.17	0.42	0.73
	ϵ_0(-)	10.11	1.25	2.15	0.77
	J(kw/m)	0.10	0.28	-0.03	0.44
	$\theta_{Jmax(degrees)}$	43.81	N/A	-0.29	0.58
	d_θ (-)	0.19	0.26	0.11	0.11

Summary of metrics for all 18 stations

Parameter	Type of statistics	RMSE	SI	Bias	R
Hs(m)					
	Mean	0.39	0.28	0.11	0.88
	Max	0.51	0.44	0.24	0.95
	Min	0.29	0.19	0.01	0.78
Te(s)					
	Mean	1.15	0.18	0.58	0.75
	Max	1.61	0.26	0.98	0.88
	Min	0.75	0.10	0.30	0.59
J(kw/m)					
	Mean	10.51	1.05	2.06	0.83
	Max	17.71	1.75	4.54	0.93
	Min	4.70	0.68	0.04	0.73
ϵ_0(-)					
	Mean	0.08	0.25	0.02	0.47
	Max	0.13	0.36	0.03	0.65
	Min	0.05	0.17	0.00	0.22
$\theta_{Jmax(degrees)}$					
	Mean	42.36	N/A	4.37	0.59
	Max	47.57	N/A	10.55	0.70
	Min	39.50	N/A	0.29	0.33
d_θ (-)					
	Mean	0.16	0.22	0.10	0.32
	Max	0.22	0.30	0.19	0.77
	Min	0.09	0.12	0.02	0.04

NDBC 41013- NC coastal

NDBC 44025- Off the NY Harbor

	Observation	Model	Observation	Model
Summer	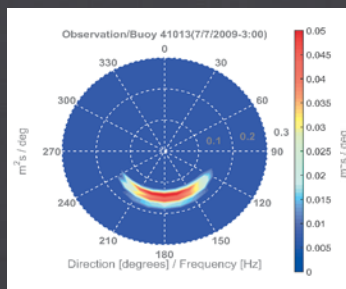	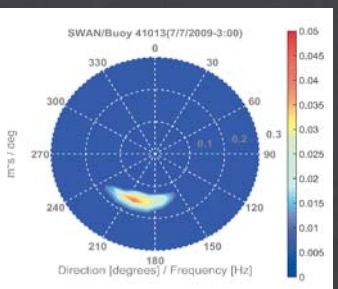	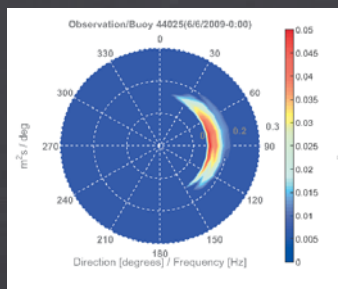	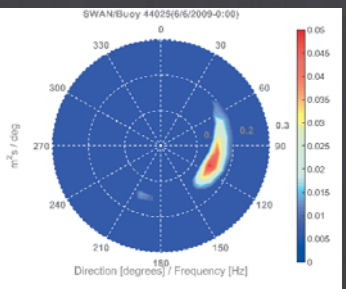
Non-Summer	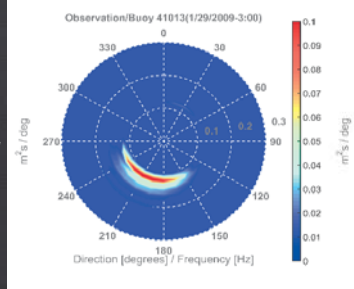	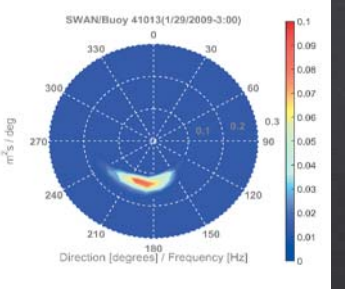	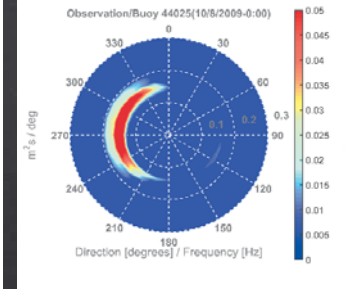	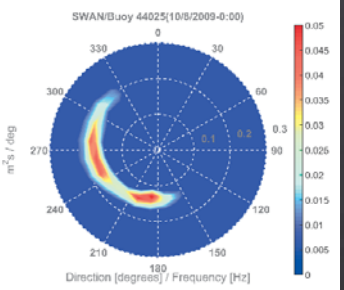

Simulated wave heights over the modeling area

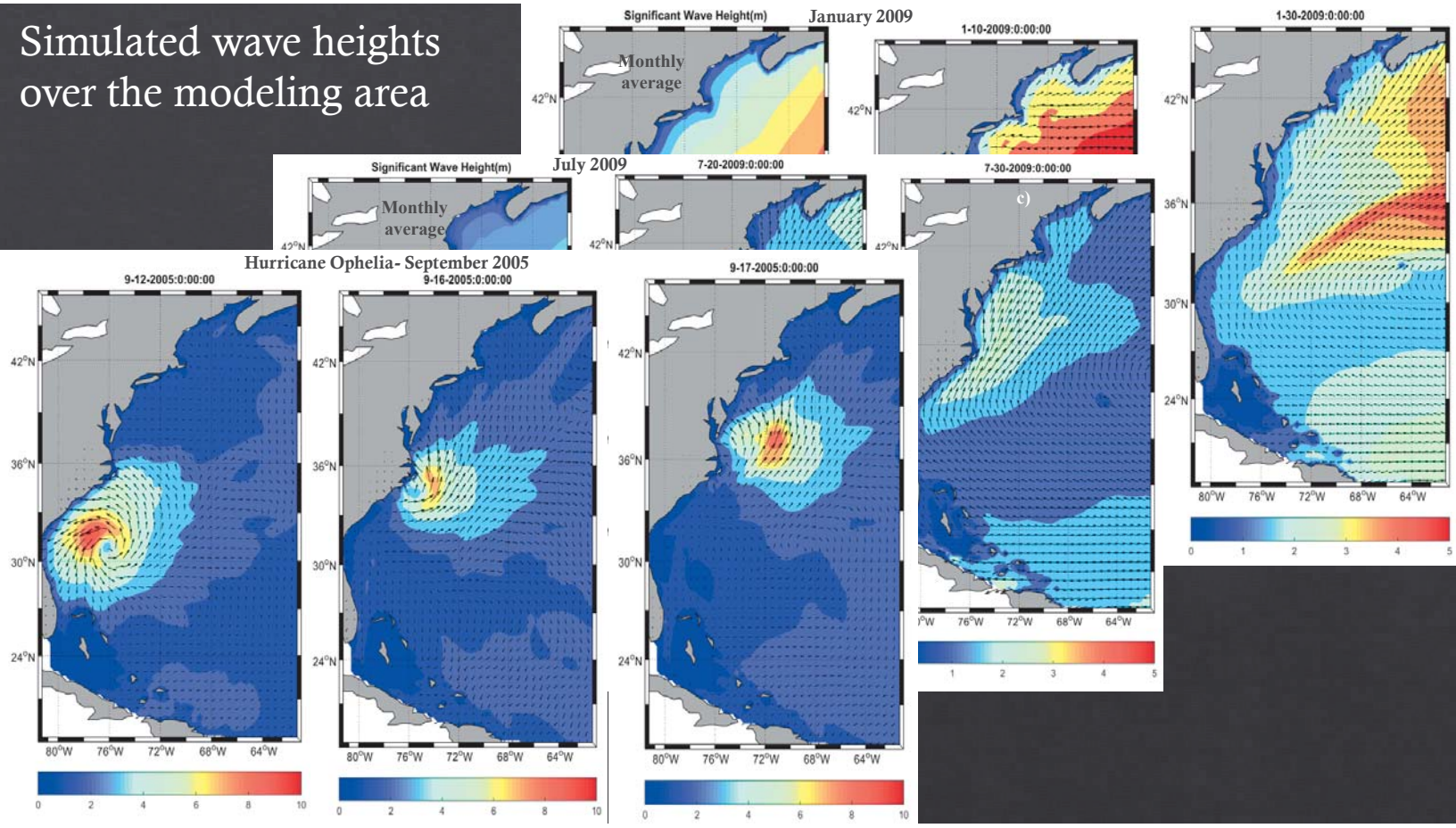

Monthly mean wave power for 2009

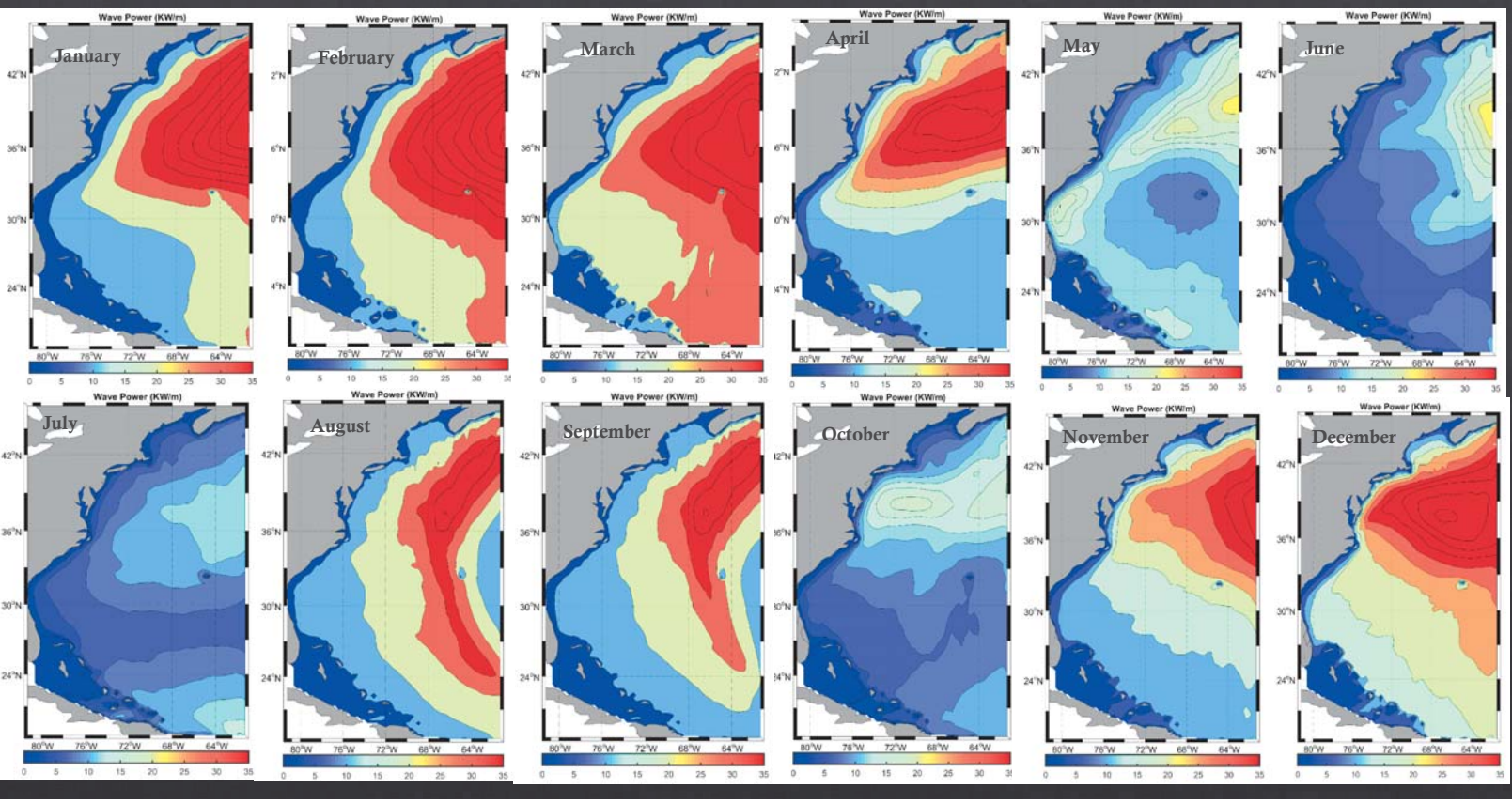

Summary and conclusions

- An ultra high-resolution wave climate model with coastal resolution of 200 meters was setup and verified
- Unstructured SWAN using a mesh with triangular elements was used
- CFSR wind field(spatial resolution of 0.312 ° and temporal resolution of 1 hour) along with WWIII-ST4(spatial resolution of 0.5 ° and temporal resolution of 3 hours) as the boundary condition were used to force the model.
- Seasonality of wind with generally higher wind speeds in winter
- Model was calibrated and verified for whitecapping dissipation
- Six IEC parameters were used for model verification
- Based on model calibration and verification results at the location of 18 NDBC buoys, Janssen(1991) with C_{ds}=2.7 δ=0.9 was selected for whitecapping dissipation. The 3-year verification results (2007-2009) were comparable with the test bed study along the West Coast
- Seasonality in wind caused seasonality in the simulated wave power with largest amounts of coastal wave power in winter and early spring and the lowest power in summer.

Acknowledgments

Sandia National Laboratories is a multi-mission laboratory managed and operated by National Technology and Engineering Solutions of Sandia LLC, a wholly owned subsidiary of Honeywell International Inc. for the U.S. Department of Energy's National Nuclear Security Administration under contract DE-NA0003525

Renewable Energy xxx (2017) 1–13

Contents lists available at ScienceDirect

Renewable Energy

journal homepage: www.elsevier.com/locate/renene

A wave model test bed study for wave energy resource characterization

Zhaoqing Yang [a, *], Vincent S. Neary [b], Taiping Wang [a], Budi Gunawan [b], Annie R. Dallman [b], Wei-Cheng Wu [a]

[a] Pacific Northwest National Laboratory, 1100 Dexter Ave North, Suite 400, Seattle, WA 98109, USA
[b] Sandia National Laboratories, P.O. Box 5800, Albuquerque, NM 87185 – MS1124, USA

ARTICLE INFO

Article history:
Received 30 August 2016
Received in revised form
20 December 2016
Accepted 22 December 2016
Available online xxx

Keywords:
Wave energy
Resource characterization
Test bed study
Numerical wave modeling
WaveWatch III
SWAN

ABSTRACT

This paper presents a test bed study conducted to evaluate best practices in wave modeling to characterize energy resources. The model test bed off the central Oregon Coast was selected because of the high wave energy and available measured data at the site. Two third-generation spectral wave models, SWAN and WWIII, were evaluated. A four-level nested-grid approach—from global to test bed scale—was employed. Model skills were assessed using a set of model performance metrics based on comparison of six simulated wave resource parameters and observations from a wave buoy inside the test bed. Both WWIII and SWAN performed well at the test bed site and exhibited similar modeling skills. The ST4 physics package with WWIII, which represents better physics for wave growth and dissipation, outperformed ST2 physics and improved wave power density and significant wave height predictions. However, ST4 physics tended to over-predict the wave energy period. The newly developed ST6 physics did not improve the overall model skill for predicting the six wave resource parameters. Sensitivity analysis using different wave frequencies and direction resolutions indicated the model results were not sensitive to spectral resolutions at the test bed site, likely due to the absence of complex bathymetric and geometric features.

1. Introduction

The recently published International Electrotechnical Commission Technical Specification (IEC TS) provides a standardized methodology for consistent and accurate wave resource assessment and characterization [1]. The methodology relies primarily on spectral wave model hindcasts for deriving recommended wave energy resource parameters. It also includes best modeling practices that depend on the desired class of wave resource characterization and assessment, including model selection, period of simulation, open boundary conditions, grid resolution, forcing (spatial and temporal) resolution, and model validation.

Although buoy observations can provide realistic directional wave spectra data for accurate resource assessment at a particular site, they are often constrained by spatial and temporal distributions. Existing buoy stations may not be close enough to the study site to be representative of the wave climate; or they may have an insufficient period of record to accurately characterize the wave climate statistics. Long-term measurement records are especially important for characterizing extreme sea states, as well as normal sea states when inter-period climate oscillations occur on the order of a few years or decades [2–6]. A minimum 10 years of record is often recommended for characterizing normal sea states, and 20 years for extreme sea states [1]. However, it is rare to find buoy observations that are representative of the wave climate at the study site and have periods of records greater than 10 years. Model hindcasts of the wave climate, therefore, offer an attractive alternative for characterizing wave energy resources [7–14].

Even if a wave model captures all of the key physics (e.g., wave generation, growth and dissipation, nonlinear interactions), accurate wave modeling still highly depends on model configurations such as source term selection and spectral resolutions, specification of forcing inputs, model grid resolutions, proper model calibration, and validation. When selecting models for wave resource characterization it is important to understand the key processes affecting wave dynamics near the shore where wave energy conversion

* Corresponding author.
E-mail address: zhaoqing.yang@pnnl.gov (Z. Yang).

http://dx.doi.org/10.1016/j.renene.2016.12.057
0960-1481/

devices are expected to be deployed. The most popular third-generation phase-averaged spectral models include the Wave Action Model (WAM) [15], Simulating WAve Nearshore (SWAN) [16], WAVEWATCH III® (WWIII) [17], TOMAWAC [18], and MIKE-21 Spectral Wave models (MIKE-21 SW) [19].

The overall goal of this study was to establish a wave model test bed to benchmark, test, and evaluate modeling methodologies and model skills for predicting the wave energy resource parameters recommended by IEC TS. The following sections review current wave modeling best practices, third-generation wave models, and evaluate model capability in predicting normal and extreme sea states, and recommend future research to improve wave modeling for resource characterization.

2. Methods

This section describes the model test bed site, the selection of wave models, and model setup, which includes data inquiries and processing, grid generation, specification of open-boundary conditions, and input configurations.

2.1. Model domain – test bed

The model test bed for wave resource characterization was selected primarily based on its meeting three criteria: 1) high wave energy resource site with potential for future wave energy converter development, 2) availability of long-term and high-quality wave measurement data, and 3) existing information from previous studies. The Oregon Coast is among the highest wave energy regions along the U.S. coasts, based on the U.S. nationwide wave resource assessment conducted by the Electric Power Research Institute [20]. Therefore, a wave modeling test bed was selected near the central Oregon Coast, approximately centered offshore from Newport, Oregon (Fig. 1). The test bed site covers an area of 44.45° – 45° N and 124.75° – 124° W (61,105 m × 59,401 m) and has annual average wave power densities that range between 35 and 50 kW/m [20]. The test bed site also includes Tier 1 wave energy converter test sites, such as the active North Energy Test Site (NETS) managed by the Pacific Marine Energy Center [10]. An operational real-time wave buoy (46050) owned and maintained by the National Oceanic and Atmospheric Administration's (NOAA's) National Data Buoy Center (NDBC) is located inside the test bed (Fig. 1). The NDBC Buoy 46050 is a 3-m discus meteorological ocean platform moored at a deep water depth of 137.2 m. The buoy station has been collecting standard meteorological data, including wind speed and direction, gust speed, air temperature, sea surface temperature since 1991, and high-quality wave spectral data since 2008.

There are some previous studies along the Oregon Coast with areas inside or overlapped with the test bed site. An initial effort was made to characterize the wave energy resource of the US Pacific Northwest by Lenee-Bluhm et al. [21] using archived spectral records from ten wave measurement buoys operated and maintained by NDBC and the Coastal Data Information Program (CDIP). García-Medina et al. [9,22] conducted a wave resource assessment along the Pacific Northwest coast using WWIII and SWAN models with a nested-grid approach. Model results from the 7-year hindcast with a 30 arc-second grid resolution were used to evaluate the temporal and spatial variability and trends of wave resource in the Pacific Northwest coast. Dallman and Neary [10] used historical data from buoy NDBC 46050 inside the test bed to present representative spectra and predict extreme sea states. Different from previous studies, the present study focuses on establishing a wave model test bed to evaluate approaches and wave models for simulating wave resource parameters recommended by IEC TS.

2.2. Wave models

A wide range of numerical models exist for simulating surface wave dynamics based on different physical assumptions and numerical frameworks. Wave models can be divided into two major categories based on different governing equations in time and frequency domains: 1) phase-resolving models and 2) phase-averaged models. Phase-resolving models are based on fundamental wave equations that involve rigorous approximations. Evolution of the sea state over time is simulated using a model grid resolution much smaller than the wavelength and fine model time step, which typically requires huge computational resources. In addition, some of the phase-resolving models, such as Boussinesq type models, are only applicable in the simulation of waves for shallow water. Therefore, phase-resolving models are impractical for hindcasts for long-term simulations (multiple years) and relatively large model domains (dimension >10 km). In contrast, phase-averaged models provide a statistical description of the wave conditions in spatial and temporal domains by solving the phase-averaged wave energy action balance equation, and they compute the distribution of wave energy in the frequency and direction domain and its evolution over time. Therefore, use of phase-averaged wave models is the most practical approach for characterizing wave resources.

Since the 1990s, third-generation wave models explicitly account for all the relevant physics for the development of ocean waves in two dimensions. WAM, WWIII SWAN, TOMWAC and MIKE-21 SM are the five most popular third-generation models that have been widely validated in many applications around the world. The present study focused on evaluation of structured-grid wave models. Among the aforementioned five third-generation wave models, TOMWAC and MIKE-21 SM are unstructured-grid models and will not be considered in the present study. WAM is very similar to WWIII and the main difference is the numerical schemes. Therefore only SWAN [16,23] and WWIII [24–26], the two most widely used third-generation, phase-averaged wave models, were evaluated in this study. Both SWAN and WWIII have been used to simulate wave climate and resource characterization around the world [9,10,13,14,20,27–32]. One of the fundamental differences between WWIII and SWAN is the numerical scheme used to solve the spectral wave action balance equation. WWIII uses explicit numerical schemes, so the model time steps are constrained by the Courant–Friedrichs–Lewy (CFL) stability criteria. SWAN uses implicit schemes, which allows much larger time steps for high computational efficiency.

WWIII was developed and is maintained by NOAA's National Centers for Environmental Prediction (NCEP) [17,25,33], as part of the marine operational forecast system. The current version of WWIII (version 4.18) consists of a collection of physics packages, including curvilinear grids, structured and unstructured-grids, effects of sea ice, and various wind-wave interaction and dissipation packages, such as the source term 2 (ST2), ST4, and ST6 physics package options [34–37]. The ST2 physics package was developed by Tolman and Chalikov [37] based on previously developed input and nonlinear interaction source terms and a new dissipation source term for low and high frequencies. The ST4 physics package consists of new parameterizations for spectral dissipation of wind-generated waves based on known properties of swell dissipation and wave breaking statistics that are consistent with observations [34]. The ST6 physics package, or the so-called BYDRZ (abbreviation for Babanin-Young-Donelan-Rogers-Zieger) source term, implements observation-based physics for wind input source term and sink terms due to negative wind input, whitecapping dissipation and wave-turbulence interactions [17,38].

In contrast to WWIII, SWAN solves the action balance equation

Please cite this article in press as: Z. Yang, et al., A wave model test bed study for wave energy resource characterization, Renewable Energy (2017), http://dx.doi.org/10.1016/j.renene.2016.12.057

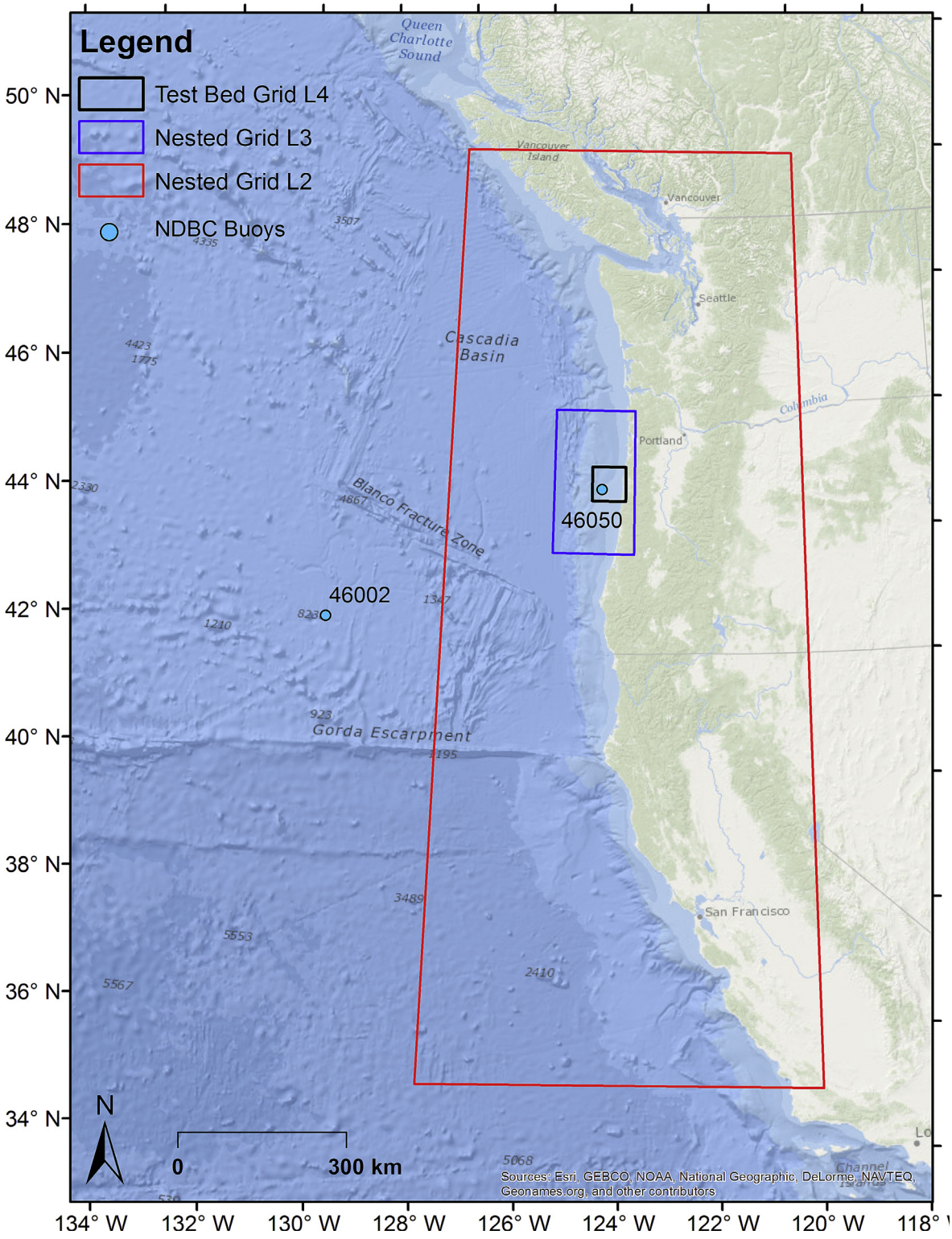

Fig. 1. Study domain and nested grids for a wave modeling test bed for resource characterization on the coast of central Oregon, USA.

using implicit numerical schemes, so it is more computationally efficient for simulating wave climate in high-resolution model grids [16]. SWAN models nearshore wave dynamics that include nonlinear wave interactions, refraction and shoaling due to bathymetry or ambient currents, and whitecapping and depth-induced breaking. In addition, SWAN can solve the steady form of the action balance equation by running in the stationary mode, which greatly reduces computational requirements and run times. This option is generally applicable when the model domain has a dimension of approximately less than 100 km [16]. As a result, SWAN is the most commonly used model for wave resource characterization in the nearshore regions [10,22,29–32,39].

Please cite this article in press as: Z. Yang, et al., A wave model test bed study for wave energy resource characterization, Renewable Energy (2017), http://dx.doi.org/10.1016/j.renene.2016.12.057

2.3. Model setup

A nested-grid approach was employed for this study. Four different levels of rectangular grids were considered. The level 1 (L1) grid is the global grid with a spatial resolution of 0.5° in both the longitudinal and latitudinal directions. The global model domain (L1) covers most of the globe from latitude 77.5° S to 77.5° N. The level 2 (L2) grid, which is nested into the global grid, covers the West Coast continental shelf (120° W to 128° W) from Southern California at 35° N to Vancouver Island, British Columbia, at 50° N. The level 3 (L3) grid centers on the Oregon Coast and is nested inside the L2 grid from 43.6° to 45.9°N and 125.6° to 123.8°W. The test bed level 4 (L4) grid is nested inside the L3 grid from 44.45° to 45°N and 124.75° to 124°W. The nested-grid scaling ratio (the ratio of the coarse-grid resolution to the fine-grid resolution) is set to a value of approximately five to six to maintain a smooth transition between model results along the nested-grid boundaries. The L2 and L3 grid resolutions are 6 arc-minutes and 1 arc-minute, respectively. The test bed (L4) grid resolution is 12 arc-seconds in the longitudinal direction and 10 arc-seconds in the latitudinal direction, which approximately corresponds to 265 m by 308 m and follows recommendations of the IEC TS [1]. The L3 grid provides open-boundary conditions for the high-resolution test bed model. In this study, estuaries and coastal bays along the coast were not considered and therefore they are not represented in the model grids. The model domains for the L4 to L2 nested grids are shown in Fig. 1. The domain coordinates (in latitude and longitude), spatial resolution (grid dimensions), and grid size (number of grid points) for all four model grids are summarized in Table 1.

Model grid and bathymetry files for the global wave model were obtained directly from NOAA's Environmental Modeling Center, Marine Modeling and Analysis Branch. The model bathymetry for the nested L2 to L4 grid was interpolated from NOAA's 3 arc-second (~90 m) Coastal Relief Model for the inner-shelf region, and NOAA's 1 arc-minute ETOPO1 Global Relief Model for the outer-shelf region and deep ocean. The resolution of the Coastal Relief Model data set is sufficient for the inner-shelf region because the local model grid resolution is ~300 m. The eastern Pacific Ocean coast has a narrow continental shelf and a deep outer-shelf basin. The model bathymetry for the test bed domain (L4) was further interpolated from NOAA's high-resolution (1/3 arc-second) tsunami bathymetry data. The average water depth for the test bed model domain is 165 m, and the maximum water depth is approximately 600 m. The distribution of model bathymetry for the test bed L4 grid is shown in Fig. 2.

Surface wind forcing is one of the most important factors for simulating wave generation and propagation from the outer continental shelf to the inner shelf; therefore, it is critical for all three classes (reconnaissance, feasibility and design) of wave resource characterization and assessment [1]. In this study, wind speed and direction were obtained from the Climate Forecast System Reanalysis (CFSR), which is a coupled atmosphere-ocean-land surface-sea ice system developed by NOAA's NCEP [40,41]. The CFSR data cover the entire global domain at a 1-h temporal resolution and a 0.5-degree spatial resolution for a 32-year period from January 1979 to March 2011. Fig. 3 shows the monthly-averaged global CFSR wind distributions in July and November 2009. A distinct seasonal pattern observed in Fig. 3 is that wind in the northern hemisphere is stronger in November (winter) than in July (summer), while opposite conditions exist in the southern hemisphere because July and November correspond respectively to winter and summer there. Sea-ice data required for the global model were also obtained from CFSR data sets. Sea-ice data have the same spatial and temporal resolutions as the wind data.

A full-year simulation allows for an evaluation of the seasonal effects on wave resource parameters. Directional spectral data at NDBC Buoy 46050 are available starting on March 5, 2008. Wave data from NDBC Buoy 46050 show strong seasonal variations of significant wave height in 2009; a series of storms occurred in winter, and relatively calm seas occurred during summer. Calendar year 2009 was selected as the model simulation period based on the availability and completeness of wind forcing data and met-ocean data for model validation at NDBC Buoy 46050. WWIII was started from 12/1/2008 to allow sufficient spin-up time.

Although tidal currents can be strong along the West Coast, especially in estuaries and bays along the Pacific Northwest coast, wave-current interaction induced by tides or ocean currents was not the focus of the study reported here. The IEC TS [1] on Wave Resource Characterization recommends including ocean current data in wave models only if depth-averaged current speeds exceed 1.5 m/s. In general, this is unlikely for points of investigation during normal sea states because the model test bed is not close to any estuaries or bays with strong currents.

3. Results and discussion

3.1. Baseline simulation

A baseline simulation was first conducted using WWIII with the ST2 physics package and SWAN in stationary mode as well as non-stationary mode (SWAN-NS). The growth and dissipation in the ST2 physics are based on the physics by Tolman and Chalikov [37]. Both WWIII and SWAN used default settings only; i.e., neither model was calibrated by tuning model parameters. The baseline simulation used 29 frequency bins with a minimum frequency of 0.035 Hz and a logarithmic increment factor of 1.1, which gives the maximum frequency of 0.505 Hz. In the directional domain, 24 direction bins were specified with a resolution of 15°. The spectral resolution meets the minimum requirements specified by IEC TS [1]; i.e., a minimum of 25 frequency components and 24 to 48 directional components, and a frequency range covering at least 0.04–0.5 Hz.

To the extent possible, the source term models for SWAN were selected to agree with those in WWIII. Common source/sink terms include those for linear wave growth by Cavaleri and Rizzoli [42], exponential wave growth by Janssen [43,44], dissipation due to bottom friction (JONSWAP [Joint North Sea Wave Project]), depth-induced breaking by Battjes and Janssen [45], and nonlinear wave-wave of quadruplets by Hasselmann et al. [46]. The formulations for the whitecapping and turbulent boundary layer dissipation are different in SWAN and WWIII (ST2). SWAN models dissipation due to whitecapping using the formulation by Komen et al. (1984), while WWIII (ST2) uses the turbulent boundary layer

Table 1
Summary of nested WWIII model grids for the wave model test bed.

Grid name	Coverage	Resolution (long., lat.)	Cell number
Global Grid L1	77°S–77°N	0.5° × 0.5° (30' × 30′)	223,920
Nested Grid L2	35°–50°N; 128°–120°W	0.1° × 0.1° (6' × 6′)	12,231
Nested Grid L3	43.6°–45.9°N; 125.6°–123.8°W	1' × 1′	15,151
Test Bed Grid L4	44.45°–45°N; 124.75°–124°W	12“ × 10” (265 m × 308 m)	44,974

Please cite this article in press as: Z. Yang, et al., A wave model test bed study for wave energy resource characterization, Renewable Energy (2017), http://dx.doi.org/10.1016/j.renene.2016.12.057

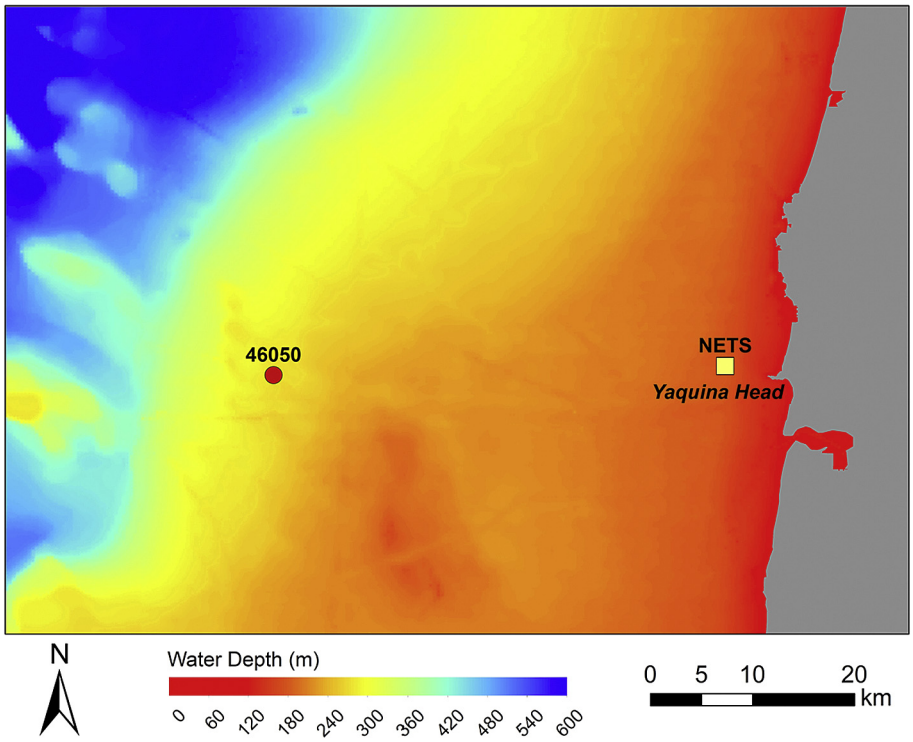

Fig. 2. Bathymetry of the test bed off central Oregon Coast. Red circle indicates the buoy location of NDBC 46050. NETS = North Energy Test Site. (For interpretation of the references to colour in this figure legend, the reader is referred to the web version of this article.)

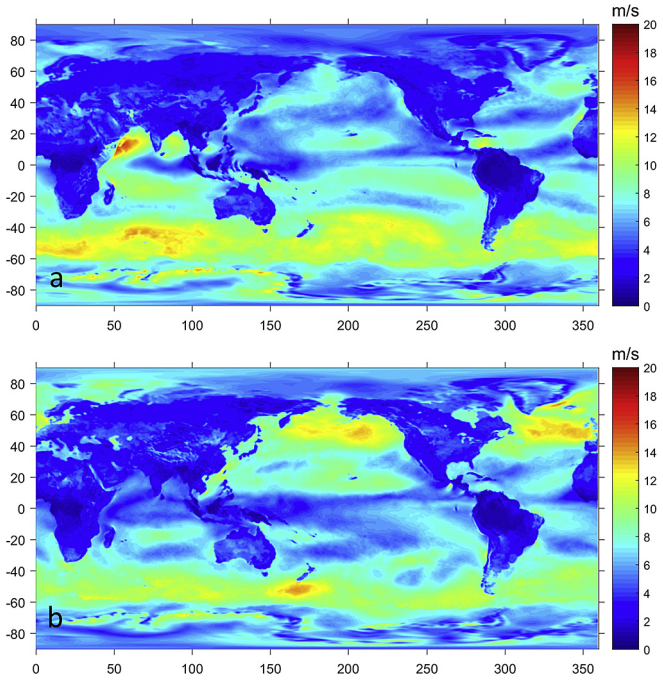

Fig. 3. Global wind distribution from the Climate Forecast System Reanalysis system at 0.5° resolution for July 2, 2009 (a) and November 7, 2009 (b).

dissipation model described by Tolman and Chalikov [37]. As noted by Tolman et al. [17], "The wind-wave growth and dissipation are separate, but interrelated processes, because the balance of these two source terms governs the integral growth characteristics of the wave model." Several combinations of these basic source terms are available in the different physics packages of WWIII, as described by Tolman et al. [17].

Both WWIII and SWAN employ source terms needed for the 'design class resource assessment' (highest resolution) in the IEC TS [1], including terms for linear and exponential wind growth, and dissipation terms that simulate whitecapping, quadruplet wave interaction, wave breaking, and bottom friction. Default parameter settings for these source term models were used in all of the simulations presented herein.

Due to different numerical schemes used in WWIII and SWAN, the model run time steps are also very different. WWIII uses a time-splitting approach with four different time steps, including the global time step Δt_g, the spatial propagation time step Δt_{xy}, the intra-spectral propagation time step Δt_k, and the source term time step Δt_s [17]. The important time step that controls model stability is the CFL time step Δt_{xy} for spatial propagation for the specific model grid resolution. The computational time step in SWAN is not restricted by CFL stability criteria, because of an implicit scheme used in the model, and one global time step is used for the model run. The time steps used in WWIII and SWAN simulations for all of the grids are shown in Table 2. Clearly, the model run time for WWIII is constrained by the small spatial propagation time step Δt_{xy} of 8 s for the test bed (L4 grid). In this study, a time step of 60 s

Table 2
Model run time steps for WWIII (L1–L4 grids) and SWAN (L4 grid).

WWIII Nested Grid	Δt_g (s)	Δt_{xy} (s)	Δt_k (s)	Δt_s (s)
Global Grid L1	3600	480	1800	30
Nested Grid L2	600	240	300	15
Nested Grid L3	100	45	50	15
Test Bed Grid L4	20	8	10	15
SWAN Grid		Δt_{xy} (s)		
Test Bed Grid L4		60		

Please cite this article in press as: Z. Yang, et al., A wave model test bed study for wave energy resource characterization, Renewable Energy (2017), http://dx.doi.org/10.1016/j.renene.2016.12.057

was used for the SWAN simulations for the test bed domain.

A year-long simulation with the nested-grid WWIII model was conducted to generate wave resource parameters for the test bed. Wave spectral data along the open boundary of the L4 grid were also outputted at hourly intervals to drive the SWAN simulation for the test bed. Fig. 4 shows the global distributions of monthly-averaged significant wave height in July and November 2009. High significant wave heights are shown in the Southern Ocean during July (Fig. 4a) and in the Eastern Pacific Ocean and Atlantic Ocean (Fig. 4b) during November, which correspond to the seasonal distribution patterns of wind field (Fig. 3). The monthly-averaged significant wave heights in the West Coast region show a smooth transition of the wave field across the nested-grid boundaries from global scale to test bed local scale (Fig. 5a and b), thereby demonstrating the successful implementation of the nested-grid approach. Significant wave heights in July in the Pacific Northwest coastal region are generally much smaller than those observed in November.

The IEC TS [1] recommends six parameters for characterizing the wave energy resource, which were used in recent studies analyzing the wave resource off the U.S. Pacific Northwest coast [9,10,21]. These six parameters are omnidirectional wave power J_{omni}, significant wave height H_{m0}, energy period T_e, spectral width $\in_0$, direction of maximum directionally resolved wave power θ, and the directionality coefficient d. The formulations of these six wave resource parameters are given in IEC TS [1], and repeated in Ref. [10]. The six IEC TS wave resource parameters were calculated based on model outputs from the baseline simulations using the WWIII ST2 physics package and SWAN. Here, only model results from WWIII are presented and compared to those calculated from buoy measurements, because the results from SWAN are similar to those from WWIII (Fig. 6). Overall, model results match the data for all six parameters quite well. Omnidirectional power, significant wave height, and energy period show strong seasonal variations. Because winds are strong in the winter and weak in the summer, omnidirectional wave power and significant wave height are large in the winter and small in the summer. The wave energy period tends to be longer as a result of the large swell caused by high wind in the winter. In contrast, the wave energy period becomes shorter in the summer because of calm sea states and low winds.

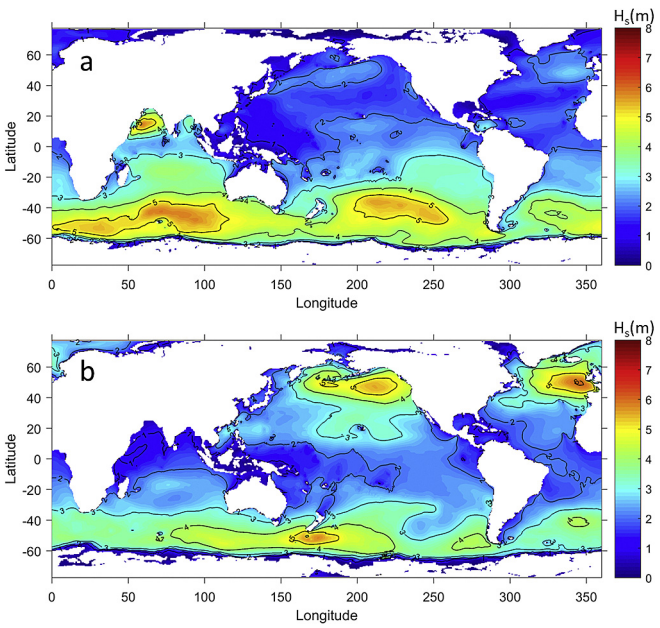

Fig. 4. Global distributions of monthly-averaged significant wave height simulated by WWIII for July 2009 (a) and November 2009 (b).

Scatter plots of the six wave resource parameters are presented in Fig. 7. In general, model results for wave power and significant wave height become more scattered and less accurate under large wave conditions (Fig. 7a and b). Simulated wave energy periods do not show strong heteroscedasticity, as do wave power J_{omini} and significant wave height H_s; rather they tend to be slightly over-predicted in comparison to observed data (Fig. 7c). Wave energy period changes from approximately 5 s during summer to as high as 15 s during winter. The spectral width generally varies between 0.2 and 0.6, with low spreading of wave energy during winter and high spreading in the summer (Fig. 7d). The wave direction of maximum directionally resolved wave power is typically in the range of 215°–315°, indicating that waves propagate dominantly from the west direction (Fig. 7e). The directional coefficient is very scattered and tends to overpredict most of the time during the year (Fig. 7f). The larger values of the directional coefficient in the winter indicate low directional spreading.

3.2. Model skills

To evaluate the performance of the model in predicting the six wave resource parameters, four statistics were computed to quantify the discrepancies between the simulated results and observed data: the root-mean-square-error, model bias, scatter index, and linear correlation coefficient. The root-mean-square-error (*RMSE*), is defined as

$$RMSE = \sqrt{\frac{\sum_{i=1}^{N}(P_i - M_i)^2}{N}}$$

where N is the number of observations, M_i is the measured value, and P_i is the predicted value.

RMSE represents the sample standard deviation of the differences between predicted values and measured values. Model bias, which represents the average difference between the predicted and measured value, is defined as

$$Bias = \frac{1}{N}\sum_{i=1}^{N}(P_i - M_i),$$

The scatter index (*SI*) is the RMSE normalized by the average of all measured values over the value of comparison:

$$SI = \frac{RMSE}{\overline{M}},$$

where the overbar indicates the mean of the measured values. The linear correlation coefficient (R) is a measure of the strength of the linear relationship between the predicted and measured values, and is defined as

$$R = \frac{\sum_{i=1}^{N}(M_i - \overline{M})(P_i - \overline{P})}{\sqrt{\left(\sum_{i=1}^{N}(M_i - \overline{M})^2\right)\left(\sum_{i=1}^{N}(P_i - \overline{P})^2\right)}}$$

The model performance metrics for each of the six IEC TS parameters are shown in Table 3 for the baseline WWIII simulation with the ST2 physics package and for the SWAN and SWAN-NS simulations with WWIII outputs as open-boundary conditions. Note that no scatter index (*SI*) values were provided for direction of maximum directionally resolved wave power θ in Table 3 because the discontinuity from 360 to 0° for the mean angle in the *SI* equation may give misleading results. The values of these model

Please cite this article in press as: Z. Yang, et al., A wave model test bed study for wave energy resource characterization, Renewable Energy (2017), http://dx.doi.org/10.1016/j.renene.2016.12.057

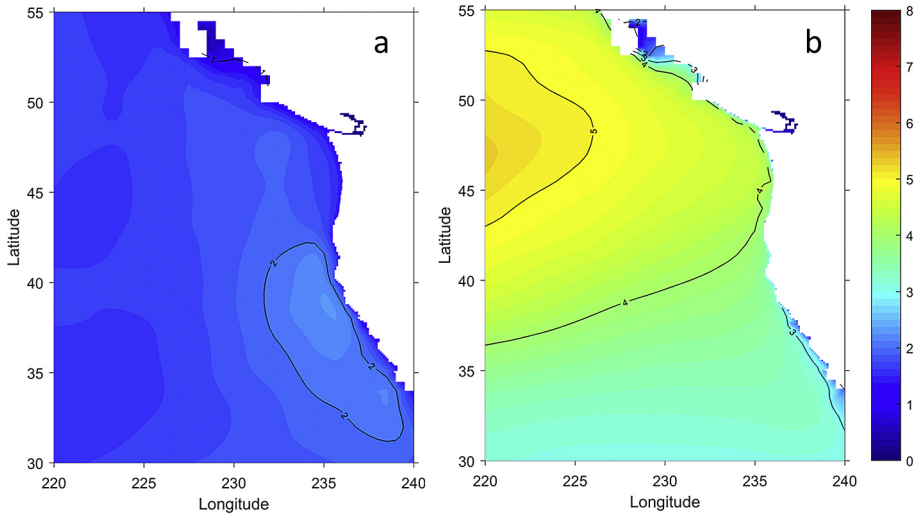

Fig. 5. Distributions of monthly-averaged significant wave height simulated by WWIII in the US West Coast region for July 2009 (a) and November 2009 (b).

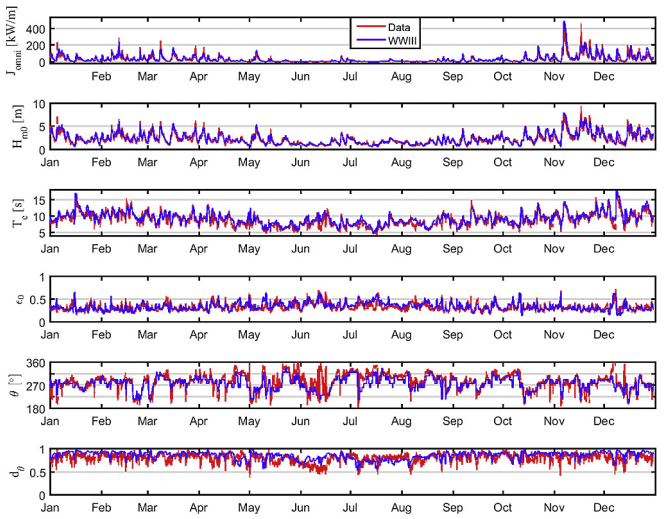

Fig. 6. Comparisons of the six IEC observed and modeled parameters at Buoy 46050 for the WWIII baseline condition.

performance metrics for all three model runs are very similar, indicating the model skills for WWIII, SWAN, and SWAN-NS are about the same at the test bed site. The error statistics for the baseline model runs are similar to those in other previous studies conducted in the region [9,22], indicating that all three models performed well and the model results are in good agreement with observations at NDBC Buoy 46050. In particular, the RMSEs for J_{omni}, H_s, and T_e are about 20.0 (kW/m), 0.42–0.45 m, and below 1 s, respectively. The linear correlation coefficients for J_{omni}, H_s, and T_e are all above 0.9. However, it is noticeable that the correlation coefficients of modeled and measured spectral width $\in_0$, direction of maximum directionally resolved wave power θ, and the directionality coefficient d are relatively low. The low correlation of $\in_0$ is because it is a function of higher order moment of variance spectrum. Therefore it is much more difficult to simulate spectral width $\in_0$. The low correlations of modeled and measured θ and d are generally due to the high uncertainty in both modeled and measured wave direction [9,12,21]. The standard accuracy required for wave direction measurement of NDBC buoys is only up to 10° [47]. Large bias in measured direction of maximum directionally resolved wave power was seen in Fig. 6, especially in June and December. Therefore, it is important to consider effects of the complexity of wave resource parameters and the uncertainty of measured data when evaluating the model skills for wave resource characterization and assessment.

3.3. Sensitivity analysis

One main difference between the WWIII and SWAN models' source term configurations is the different treatment of wave growth and dissipation. The recent development of new physical packages in WWIII, such as ST4 and ST6 physics, has improved model prediction for different growth and dissipation processes, including swell dissipation [17,24,34,38,48]. Sensitivity analysis was conducted to evaluate the effects of the ST4 and ST6 physics package on wave climate.

In the WWIII ST4 physics package, the swell dissipation is estimated based on global satellite Synthetic Aperture Radar data and a combination of a viscous and turbulent boundary layer [24]. In the ST4 sensitivity run, the ST4 physics package was turned on in all four WWIII nested grids. However, model configurations for the SWAN-ST4 run remained the same as the baseline stationary run except that open-boundary conditions were specified with outputs from the WWIII-ST4 simulation along the boundary grid points of the L4 domain.

To evaluate the performance of the ST4 physics package in comparison to the baseline simulations with the ST2 physics package, the four error statistics for the six IEC TS wave resources were calculated based on the ST4 WWIII and SWAN simulations and are shown in Table 4. Compared to model performance metrics with the ST2 physics package (Table 3), simulations using WWIII and SWAN with the ST4 physics package show better model skills for predicting wave power J_{omni} and significant wave height H_s. Improvement in model accuracy for WWIII-ST4 is clearly seen to be greater than that for SWAN-ST4. This is simply because the ST4 physics package was activated in all four domains for the WWIII-ST4 simulation, while the SWAN-ST4 simulation was only forced with WWIII-ST4 outputs along the L4 domain boundary. The model skills using ST4 for predicting wave energy period T_e, however, were worse than those using ST2. The RMSEs for energy period were increased by about 25%, from below 1 s to greater than 1.2 s. Error statistics for the other three resource parameters ($\in_0$, θ and $d\theta$) are about the same for the ST2 and ST4 physics packages

Please cite this article in press as: Z. Yang, et al., A wave model test bed study for wave energy resource characterization, Renewable Energy (2017), http://dx.doi.org/10.1016/j.renene.2016.12.057

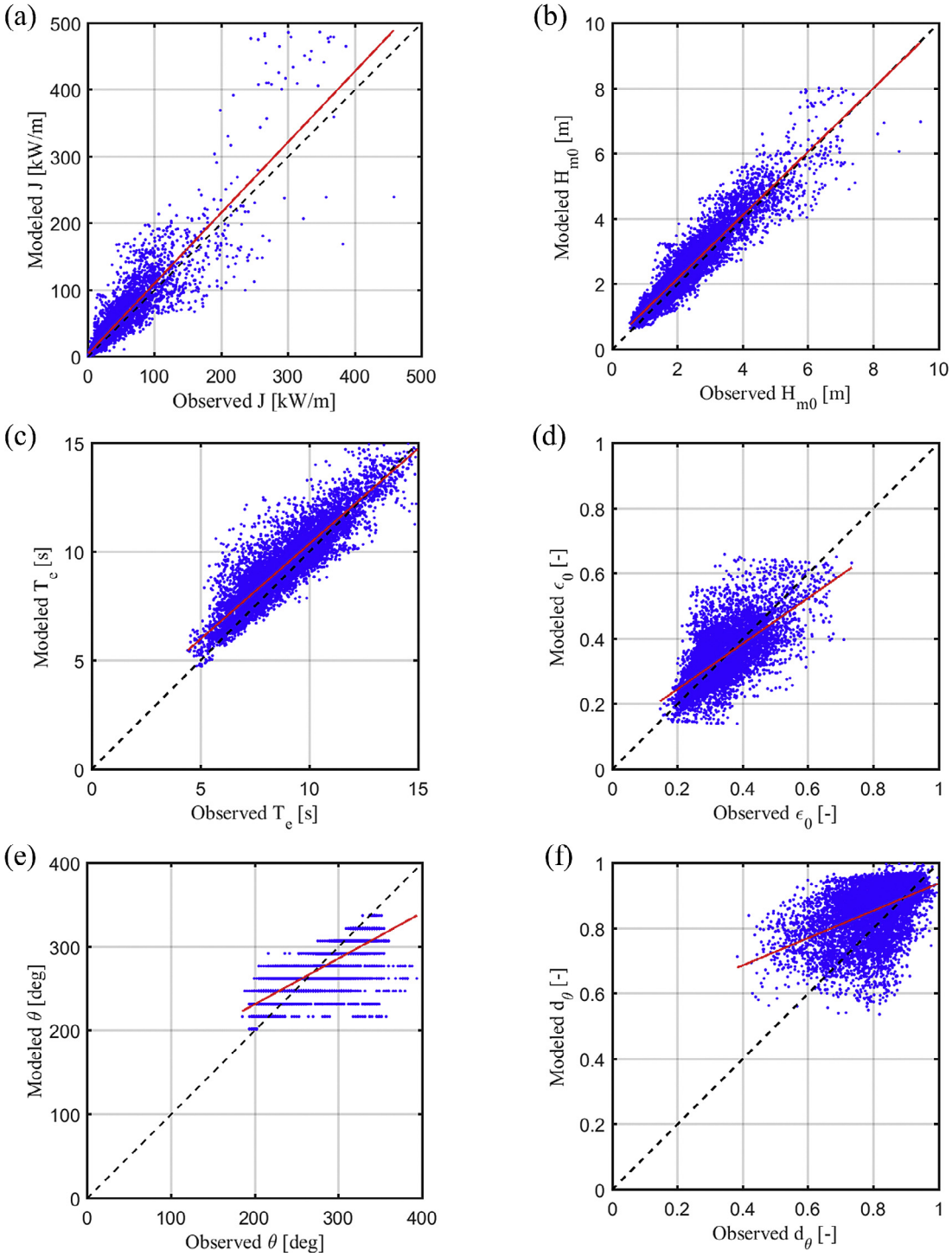

Fig. 7. Scatter plots of the six IEC observed and modeled wave resource parameters using the WWIII model with the ST2 physics package. The red line is the linear regression. The black dash line represents the locus of where predicted and observed values are the same. (For interpretation of the references to colour in this figure legend, the reader is referred to the web version of this article.)

(Tables 3 and 4).

A sensitivity run with WWIII using ST6 physics was also conducted. Error statistics for model simulation with WWIII ST6 was calculated and given in Table 4. Clearly, the ST6 physics did not improve the overall model skills for simulating the six IEC TS wave resources parameters compared to the baseline simulation with ST2 physics. Similar to ST4 physics, ST6 predicted better omnidirectional wave power than ST2. However, error statistics with ST6 physics for other parameters were slightly worse than those with ST2 and ST4 physics.

To further evaluate the differences in the performance of the ST2 and ST4 physics packages, comparisons of significant wave heights between observed data and modeled results using the ST2 and ST4 physics packages are plotted for July and November 2009, representing the summer and winter conditions, respectively (Fig. 8). In July when the sea state was calm, the differences between ST2 and

Please cite this article in press as: Z. Yang, et al., A wave model test bed study for wave energy resource characterization, Renewable Energy (2017), http://dx.doi.org/10.1016/j.renene.2016.12.057

Table 3
Performance metrics for baseline simulations.

Parameter	Model	RMSE	SI	Bias	R
J (kW/m)	WWIII	20.0	0.64	6.1	0.91
	SWAN	20.0	0.63	6.5	0.91
	SWAN-NS	19.0	0.62	6.3	0.91
H_s (m)	WWIII	0.42	0.19	0.16	0.94
	SWAN	0.45	0.20	0.19	0.94
	SWAN-NS	0.44	0.20	0.18	0.94
T_e (s)	WWIII	0.98	0.11	0.50	0.90
	SWAN	0.96	0.11	0.51	0.91
	SWAN-NS	0.95	0.11	0.52	0.91
ε_0 (−)	WWIII	0.07	0.20	0.01	0.68
	SWAN	0.07	0.20	0.00	0.71
	SWAN-NS	0.06	0.19	0.00	0.72
θ (degrees)	WWIII	22.87	n/a	−6.87	0.74
	SWAN	22.62	n/a	−6.65	0.74
	SWAN-NS	22.24	n/a	−6.62	0.75
d_θ (−)	WWIII	0.10	0.13	0.05	0.48
	SWAN	0.10	0.12	0.04	0.55
	SWAN-NS	0.10	0.12	0.04	0.55

Table 4
Performance metrics for sensitivity runs with the ST4 and ST6 physics package.

Parameter	Model	RMSE	SI	Bias	R
J (kW/m)	SWAN-ST4	17.12	0.55	3.20	0.91
	WWIII-ST4	16	0.51	2.0	0.92
	WWIII-ST6	16	0.52	−1.5	0.91
H_s (m)	SWAN-ST4	0.43	0.19	0.07	0.93
	WWIII-ST4	0.38	0.17	0.01	0.94
	WWIII-ST6	0.43	0.19	−0.11	0.93
T_e (s)	SWAN-ST4	1.20	0.13	0.79	0.89
	WWIII-ST4	1.23	0.14	0.86	0.90
	WWIII-ST6	1.35	0.15	0.88	0.85
ε_0 (−)	SWAN-ST4	0.07	0.21	0.01	0.67
	WWIII-ST4	0.07	0.20	0.01	0.65
	WWIII-ST6	0.08	0.25	0.02	0.53
θ (degrees)	SWAN-ST4	23.08	n/a	−7.33	0.73
	WWIII-ST4	23.44	n/a	−7.62	0.73
	WWIII-ST6	29.64	n/a	−12.49	0.57
d_θ (−)	SWAN-ST4	0.10	0.12	0.04	0.51
	WWIII-ST4	0.10	0.13	0.05	0.54
	WWIII-ST6	0.11	0.14	0.03	0.28

ST4 results were small. However, in November, when large swells were present, using the ST4 physics package improved the model skill in predicting the peak wave height and timing of large waves, because of the better ST4 representation of peak frequency. Monthly distributions of RMSEs for J_{omni} and H_s with ST2 and ST4 physics are shown in Fig. 9. Seasonal variations in RMSEs for J_{omni} and H_s are evident; low RMSE values occurred in the summer and high values in the winter. The RMSEs with ST4 simulations are similar to those with ST2 simulations in the summer, but smaller in the winter, indicating that the ST4 physics package performs better at simulating swell growth and dissipation. Cumulative frequency distributions of significant wave heights calculated based on observations and modeled results using the ST2 and ST4 physics packages are presented in Fig. 10. Again, the cumulative frequency distribution when using ST4 is significantly better than ST2 in comparison to field observations, especially for significant wave heights greater than 1.5 m, which once again indicates ST4 physics is better at simulating large waves than ST2 physics.

To better understand the effect of ST4 physics on simulating wave climate in the frequency and directional domain, two-dimensional wave energy spectra were calculated based on observations and model results using ST2 and ST4 physics for July 15, 2009 (Fig. 11) and November 22, 2009 (Fig. 12), respectively. Although at a broader scale distribution patterns of wave energy spectra with ST2 and ST4 physics are consistent with observations, dominant energy propagates from the northwest in July and from the southwest in November, and ST4 physics showed overall better performance in producing the wave energy spectra. ST4 physics predicted dominant spectra in the direction ranging from 300 to 350° (Fig. 11b) in July, which is similar to the observation in the range from 300 to 360° (Fig. 11c), while ST2 physics predicted the wave spectra in a narrower range from 315 to 340° (Fig. 11a). ST2 physics also overpredicted the peak frequency at 0.21 Hz, while ST4 and observations both showed a peak frequency below 0.2 Hz. Similarly, ST4 showed greater skill in predicting the direction range of peak spectra and the peak magnitude in comparison to observations in November (Fig. 12).

Although the configurations of frequency and direction resolution specified in the baseline simulations met the minimum requirement recommended in the IEC TS [1], higher spectral resolution, both in frequency and direction, generally has the potential to improve model prediction of energy advection from swell over long distances. In particular, complex geometry and bathymetry in shallow-water regions will alter the frequency-directional characteristic of incoming waves. However, increasing the spectral resolution in frequency and direction will also proportionally increase the computational time. Therefore, it is useful to assess the balance of model prediction accuracy versus computational cost.

Sensitivity model runs were conducted using the WWIII model by varying the number of frequency and direction bins to evaluate the effect of frequency and direction resolutions on the accuracy of wave prediction. The number of frequency bins was increased from 29 to 50; with a 1.07 logarithmic increment factor and a minimum frequency of 0.035 Hz, the maximum frequency is nearly 1 Hz at 0.96 Hz. The number of directional bins was increased from 24 (15-degree resolution) to 36 (10-degree resolution).

A time-series comparison of the predicted significant wave height from WWIII and SWAN models with finer spectral resolution results from the baseline model, and observations at NDBC Buoy 46050 show that increasing the spectral resolution provides no improvement in WWIII and SWAN model skill. Model insensitivity to spectral resolution in this study was likely due to the large water depth (128 m) and the absence of any bathymetric or geometric features at the point of comparison (NDBC Buoy 46050). However, wave models may be sensitive to spectral resolutions at other locations that have complex geometry features and shallow-water depths.

3.4. Computation efficiency

One of the common challenges in modeling is the significant computational resources needed to perform model simulations of wave climates at a high resolution. Because the WWIII and SWAN models use very different numerical schemes, their requirements for computational platforms and simulation times are also different. The SWAN simulation requirements assume 16-core CPU platforms, which are widely available at a reasonable cost. SWAN simulations in the present study were performed using 16-core RHEL 6.4 Linux-based operating system platforms with Intel Xeon E7-4880 processors rated at 2.5 GHz clock speeds, with 37.5 MB of L3 Cache, and 1 TB of RAM. The WWIII simulations were performed using 8 nodes on a supercomputer consisting of 692 nodes. Each node is dual socket with 16 cores per socket and an AMD Interlagos processor running at 2.1 GHz with 64 GB of 1600 MHz memory per node (2 GB/socket).

Table 5 provides a summary of the computational times for WWIII and SWAN in both stationary and non-stationary modes. These results indicate that the computation time requirement for WWIII is significantly greater than it is for SWAN in stationary

Please cite this article in press as: Z. Yang, et al., A wave model test bed study for wave energy resource characterization, Renewable Energy (2017), http://dx.doi.org/10.1016/j.renene.2016.12.057

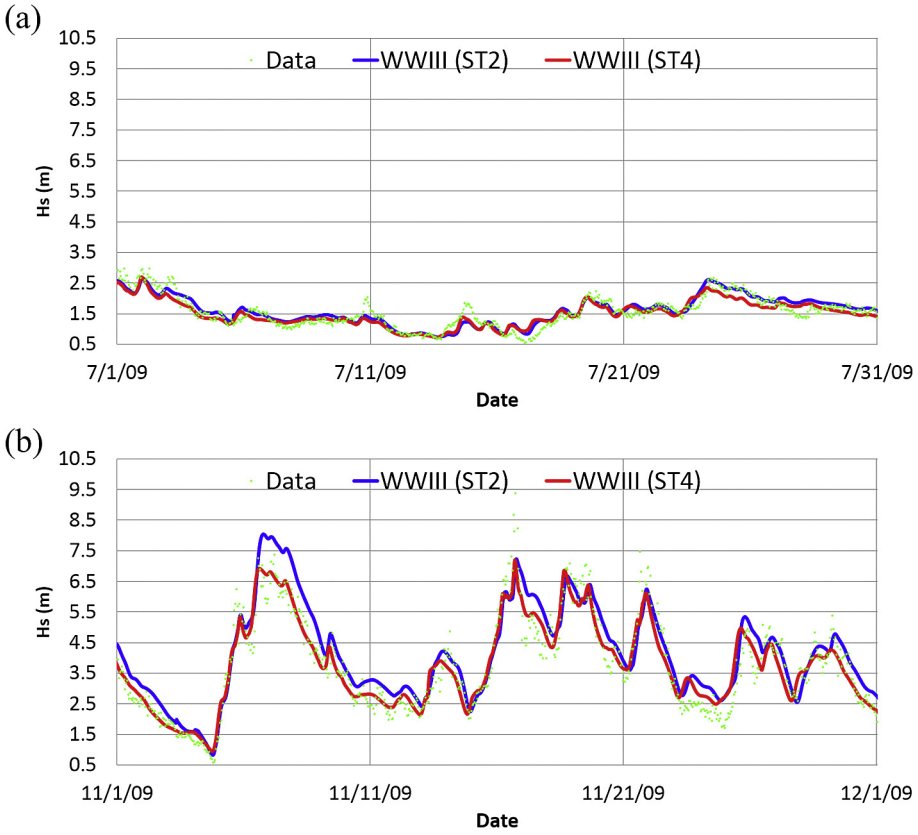

Fig. 8. Comparisons of the observed and modeled significant wave heights at Buoy 46050 using the WWIII ST2 and ST4 physics packages for July (a) and November (b) 2009.

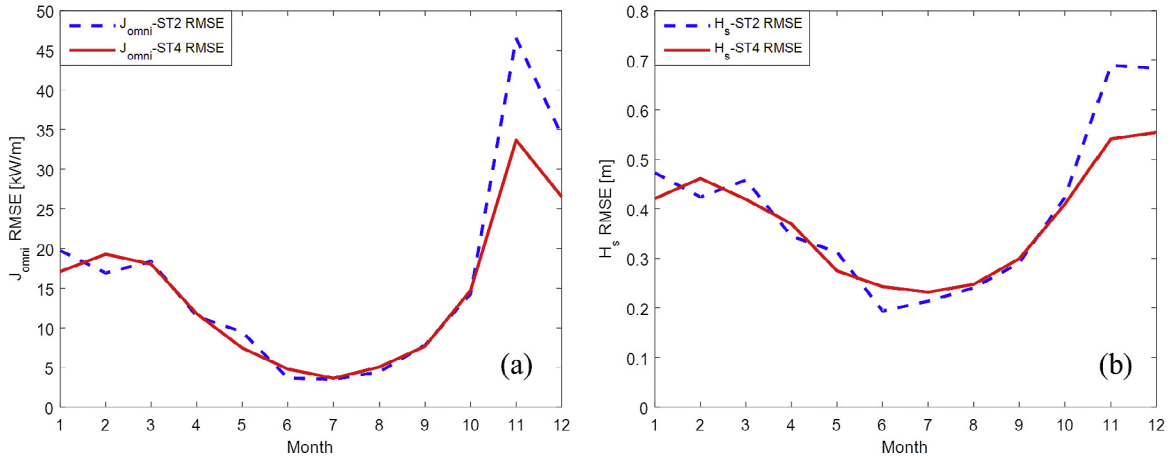

Fig. 9. Monthly RMSEs of omnidirectional J_{omni} (a) and significant wave height H_s (b) of WWIII simulations with ST2 and ST4 physics at Buoy 46050.

mode, although WWIII runs included all four-nested grids. Even performing runs on a cluster using 256 cores, it took more than 5 days to complete a 1-year simulation using WWIII. In contrast, SWAN, in stationary mode, took less than 2 days to complete a 1-year simulation on a 16-core CPU platform, which shows great efficiency over WWIII. CPU hours increased significantly, nearly 19 times, when modeling the unsteady-state term in the action balance equation using the non-stationary mode of SWAN. As expected, a significant increase in CPU hours was observed when increasing the spectral resolution, proportional to the ratio of increase in resolution.

4. Summary and conclusions

A wave model test bed off the central Oregon Coast was established to evaluate the performance of third-generation, phase-averaged spectral wave models and different modeling approaches for simulating the six wave energy resource parameters recommended by IEC TS [1]. The overarching goal of the test bed study was to provide industry with guidance for model selection and modeling best practices, depending on the wave site conditions and desired class of wave resource assessment. This paper presents the results from the initial effort of the test bed study to evaluate two of the most widely used third-generation spectral models, WWIII and

Please cite this article in press as: Z. Yang, et al., A wave model test bed study for wave energy resource characterization, Renewable Energy (2017), http://dx.doi.org/10.1016/j.renene.2016.12.057

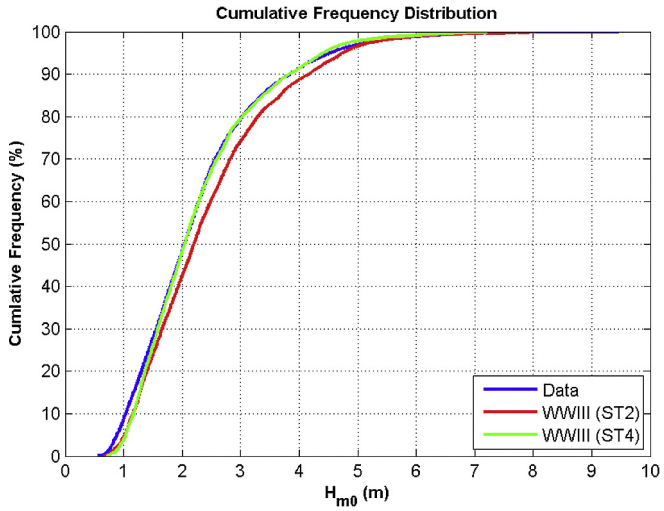

Fig. 10. Cumulative frequency distributions of significant wave heights derived from observations and WWIII simulations at Buoy 46050.

SWAN, and the nested-grid modeling approach that uses a structured-grid framework.

A nested structured-grid approach, with three levels of outer grids, was employed to provide open-boundary conditions for the test bed domain (L4). The three outer grids included the global domain as the outermost grid (L1), the Pacific Northwest coastal region as the second-level outer grid (L2) nested within L1 grid, and the central Oregon Coast as the third outer grid (L3) nested within L2 grid. For WWIII simulations, all four-level models were two-way nesting and run at the same time. The SWAN model for the test bed domain was driven by WWIII outputs from the L3 domain (one-way nesting). The four-level nested-grid modeling framework, using NOAA's WWIII global model as the lowest-level model, provides an accurate and efficient approach that is suitable for the feasibility class resource assessment at a spatial resolution of ~300 m.

Table 5
Summary of WWIII and SWAN computational times for the baseline simulation.

Model Run	Description	Clock Time	Total CPU-hour
WWIII[b]	Baseline	5.1 days	31,488
SWAN-S[a]	Baseline, Stationary	1.9 days	731
SWAN-NS[a]	Baseline, Non-stationary	35.3 days	13,572

[a] Model run time on a 16-core CPU platform.
[b] Model run time on a cluster using 256 cores (8 nodes with 32-core per node).

Model performance was evaluated using standard performance metrics based on a comparison of predictions of six IEC wave resource parameters derived by model hindcasts to those derived from buoy measurements. Comparisons of baseline model results derived from WWIII and SWAN to observed data for the six IEC parameters indicate good agreement between model simulations and buoy measurements. Differences between WWIII and SWAN predictions at the NDBC Buoy 46050 location were negligible. Better representations of growth and dissipation using ST4 physics in the WWIII model generally improved model performance. Notably, model skill for predicting omnidirectional wave power density and significant wave height for large waves, which are important for wave resource assessment, was significantly improved with ST4 physics. In contrast, model skill for predicting energy period was slightly reduced with the ST4 physics. Sensitivity analysis with WWIII ST6 physics indicated that the ST6 physics did not improve the model performance in predicting the six IEC TS wave resource parameters at the test bed site. Therefore, use of ST4 physics is recommended for wave resource assessment, even if the WWIII model is used to provide open-boundary conditions.

Sensitivity analysis also indicated that increasing the spectral resolution in both frequency and direction domains provided no improvement in WWIII or SWAN model skills, suggesting that in the area with relatively smooth bathymetry and coastlines, spectral resolution with 29 frequency bins and 24 directional bins may be sufficient. However, this insensitivity was likely due to the large water depth (128 m) at the point of comparison and the absence of any complex bathymetric or geometric features in the vicinity.

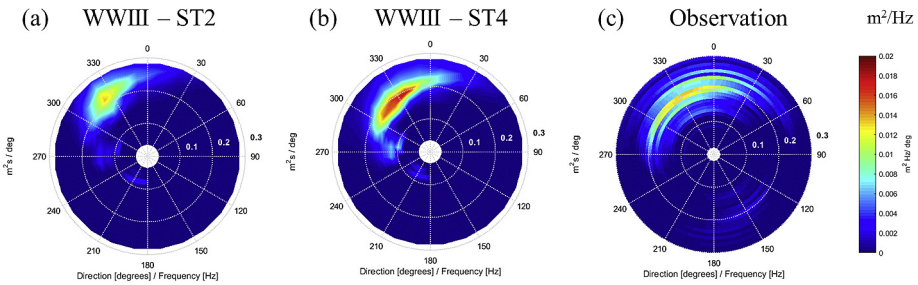

Fig. 11. Distributions of 2D wave energy spectra computed using WWIII with ST2 physics (a), ST4 physics (b), and observation data (c) on July 15, 2009.

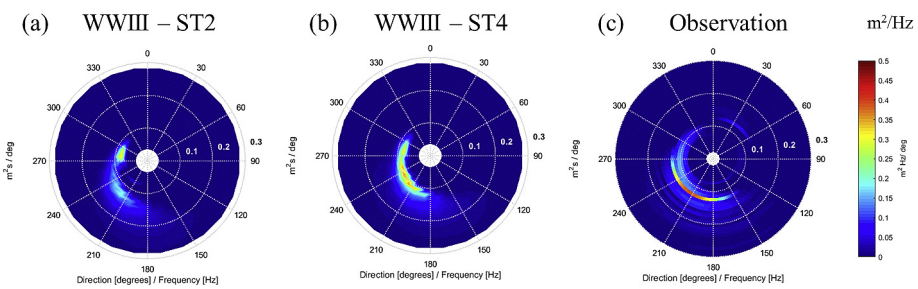

Fig. 12. Distributions of 2D wave energy spectra computed from WWIII with ST2 physics (a), ST4 physics (b) and observation data (c) on November 22, 2009.

Please cite this article in press as: Z. Yang, et al., A wave model test bed study for wave energy resource characterization, Renewable Energy (2017), http://dx.doi.org/10.1016/j.renene.2016.12.057

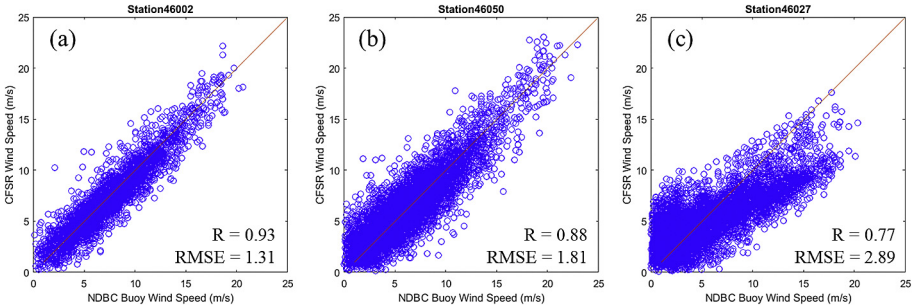

Fig. 13. Comparison of observed and CFSR-predicted winds at NDBC buoy station 46002 (a), 46050 (b), and 46027 (c).

One of the most important factors that affect model accuracy is surface wind forcing, particularly for large wave prediction. The PNW coast is dominated by strong winds and swells in the winter months, as shown in Fig. 5. However, CFSR winds are generally underpredicted in the winter, which is likely the cause of underestimate of the swell peaks (Fig. 8). Fig. 13 shows the comparison of observed and CFSR-predicted winds at NDBC 46002 in the deep open ocean at a water depth of 3,368 m, NBDC 46050 at the inner shelf (also in the test bed) at 128 m, and station 46027 in the nearshore at a shallow-water depth of 46 m (see locations in Fig. 1). Clearly, the accuracy of CFSR-predicted wind speed decreases gradually as the locations become close to the shore. CFSR wind speed prediction matches observations the best at NDBC 46002, with a RMSE of 1.31 (m/s) and linear correlation coefficient R of 0.93. The RMSE and R are 1.81 (m/s) and 0.88 for NDBC 46050, and 2.89 (m/s) and 0.77 for NDBC 46027, respectively. Therefore, improvement in wind prediction capability, especially in the nearshore region, is important for wave resource characterization [49,50]. The present study was limited to evaluation of a structured-grid model skill at a deep offshore site in a northwest wave climate with default model settings. Future studies should include the evaluation of model performance in shallow-water environments, unstructured-grid models, and potential improvement in model predictions of wave energy periods for large waves.

Acknowledgements

This study was funded by the Wind and Water Power Technologies Office within the Office of Energy Efficiency and Renewable Energy, U.S. Department of Energy under contract DE-AC05-76RL01830 to Pacific Northwest National Laboratory and contract DE-AC04-94AL8500 to Sandia National Laboratories. The authors thank members of a steering committee charged with external review of this study, including Tuba Ozkan-Haller of Oregon State University, who served as chairperson, Bryson Robertson of the Institute of Energy Systems at the University of Victoria, Arun Chawla from NCEP at NOAA, Tim Mundon from Oscilla Power™, Inc., and Levi Kilcher from the National Renewable Energy Laboratory.

References

[1] IEC, Marine energy – Wave, Tidal and Other Water Current Converters – Part 101: Wave Energy Resource Assessment and Characterization, International Electrotechnical Commission, Geneva, Switzerland, 2015.
[2] X.L.L. Wang, V.R. Swail, Changes of extreme wave heights in Northern Hemisphere oceans and related atmospheric circulation regimes, J. Clim. 14 (10) (2001) 2204–2221.
[3] S.M. Brooks, T. Spencer, A. McIvor, I. Moller, Reconstructing and understanding the impacts of storms and surges, southern North Sea, Earth Surf. Process. Landforms 41 (6) (2016) 855–864.
[4] P.D. Bromirski, D.R. Cayan, Wave power variability and trends across the North Atlantic influenced by decadal climate patterns, J. Geophys. Res. Oceans 120 (5) (2015) 3419–3443.
[5] S. Caires, A. Sterl, 100-year return value estimates for ocean wind speed and significant wave height from the ERA-40 data, J. Clim. 18 (7) (2005) 1032–1048.
[6] I. Grabemann, N. Groll, J. Moller, R. Weisse, Climate change impact on North Sea wave conditions: a consistent analysis of ten projections, Ocean. Dyn. 65 (2) (2015) 255–267.
[7] R. Carballo, M. Sanchez, V. Ramos, F. Taveira-Pinto, G. Iglesias, A high resolution geospatial database for wave energy exploitation, Energy 68 (2014) 572–583.
[8] A. Chawla, D.M. Spindler, H.L. Tolman, Validation of a thirty year wave hindcast using the Climate Forecast System Reanalysis winds, Ocean. Model. 70 (2013) 189–206.
[9] G. García-Medina, H.T. Özkan-Haller, P. Ruggiero, Wave resource assessment in Oregon and southwest Washington, USA, Renew. Energy 64 (2014) 203–214.
[10] A.R. Dallman, V.S. Neary, Characterization of U.S. Wave Energy Converter (WEC) Test Sites: a Catalogue of Met-ocean Data, second ed., Sandia National Laboratories, Albuquerque, New Mexico, 2015.
[11] B. Liang, F. Fan, F. Liu, S. Gao, H. Zuo, 22-Year wave energy hindcast for the China East Adjacent Seas, Renew. Energy 71 (2014) 200–207.
[12] B.R.D. Robertson, C.E. Hiles, B.J. Buckham, Characterizing the near shore wave energy resource on the west coast of Vancouver Island, Canada, Renew. Energy 71 (2014) 665–678.
[13] W.E. Rogers, J.M. Kaihatu, L. Hsu, R.E. Jensen, J.D. Dykes, K.T. Holland, Forecasting and hindcasting waves with the SWAN model in the Southern California Bight, Coast. Eng. 54 (1) (2007) 1–15.
[14] N. Li, K.F. Cheung, J.E. Stopa, F. Hsiao, Y.L. Chen, L. Vega, P. Cross, Thirty-four years of Hawaii wave hindcast from downscaling of climate forecast system reanalysis, Ocean. Model. 100 (2016) 78–95.
[15] WAMDI, The WAM model – a third generation ocean wave prediction model, J. Phys. Oceanogr. 18 (12) (1988).
[16] SWAN, SWAN: User Manual, Cycle III Version 41.01A, Delft University of Technology, Delft, The Netherlands, 2015.
[17] H.L. Tolman, WAVEWATCH III Development Group, User Manual and System Documentation of Wavewatch III® Version 4.18, National Oceanic and Atmospheric Administration, National Weather Service, National Centers for Environmental Prediction, College Park, MD 20740, 2014, p. 311.
[18] M. Benoit, F. Marcos, F. Becq, TOMAWAC: a prediction model for offshore and nearshore storm waves, in: Environmental and Coastal Hydraulics: Protecting the Aquatic Habitat, Proceedings of Theme B, Vols 1 & 2, 1997, pp. 1316–1321, 27.
[19] DHI, Mike 21 Spectral Waves FM – Short Description, DHI, Horsholm Denmark, 2012, p. 16.
[20] EPRI, Mapping and assessment of the United States ocean wave energy resource, in: EPRI 2011 Technical Report to U.S. Department of Energy, Electric Power Research Institute, Palo Alto, California, 2011.
[21] P. Lenee-Bluhm, R. Paasch, H.T. Ozkan-Haller, Characterizing the wave energy resource of the US Pacific Northwest, Renew. Energy 36 (8) (2011) 2106–2119.
[22] G. García-Medina, H.T. Özkan-Haller, P. Ruggiero, J. Oskamp, An inner-shelf wave forecasting system for the U.S. pacific northwest, Weather Forecast. 28 (3) (2013) 681–703.
[23] N. Booij, R.C. Ris, L.H. Holthuijsen, A third-generation wave model for coastal regions – 1. Model description and validation, J. Geophys. Res. Oceans 104 (C4) (1999) 7649–7666.
[24] F. Ardhuin, B. Chapron, F. Collard, Observation of swell dissipation across oceans, Geophys. Res. Lett. 36 (6) (2009).
[25] H.L. Tolman, A new global wave forecast system at NCEP, Ocean Wave Meas. Anal. 1 and 2 (1998) 777–786.
[26] A. Chawla, H.L. Tolman, V. Gerald, D. Spindler, T. Spindler, J.H.G.M. Alves, D.G. Cao, J.L. Hanson, E.M. Devaliere, A multigrid wave forecasting model: a new paradigm in operational wave forecasting, Weather Forecast. 28 (4) (2013) 1057–1078.
[27] B.C. Liang, X. Liu, H.J. Li, Y.J. Wu, D.Y. Lee, Wave climate hindcasts for the Bohai Sea, Yellow Sea, and East China Sea, J. Coast. Res. 32 (1) (2016) 172–180.

Please cite this article in press as: Z. Yang, et al., A wave model test bed study for wave energy resource characterization, Renewable Energy (2017), http://dx.doi.org/10.1016/j.renene.2016.12.057

[28] M.A. Hemer, D.A. Griffin, The wave energy resource along Australia's Southern margin, J. Renew. Sustain. Energy 2 (4) (2010) 043108.
[29] G. Chang, K. Ruehl, C.A. Jones, J. Roberts, C. Chartrand, Numerical modeling of the effects of wave energy converter characteristics on nearshore wave conditions, Renew. Energy 89 (2016) 636–648.
[30] N. Guillou, G. Chapalain, Numerical modelling of nearshore wave energy resource in the Sea of Iroise, Renew. Energy 83 (2015) 942–953.
[31] M. Monteforte, C. Lo Re, G.B. Ferreri, Wave energy assessment in Sicily (Italy), Renew. Energy 78 (2015) 276–287.
[32] D. Silva, A.R. Bento, P. Martinho, C.G. Soares, High resolution local wave energy modelling in the Iberian Peninsula, Energy 91 (2015) 1099–1112.
[33] H.L. Tolman, A generalized multiple discrete interaction approximation for resonant four-wave interactions in wind wave models, Ocean. Model. 70 (2013) 11–24.
[34] F. Ardhuin, E. Rogers, A.V. Babanin, J.-F. Filipot, R. Magne, A. Roland, A. van der Westhuysen, P. Queffeulou, J.-M. Lefevre, L. Aouf, F. Collard, Semiempirical dissipation source functions for ocean waves. Part I: definition, calibration, and validation, J. of Physical Oceanography 40 (9) (2010) 1917–1941.
[35] H.L. Tolman, Treatment of unresolved islands and ice in wind wave models, Ocean. Model. 5 (3) (2003) 219–231.
[36] A. Roland, Development of WWM II: Spectral Wave Modelling on Unstructured Meshes, Institute of Hydraulic and Water Resources Engineering, 2009 (Technische Universitat Darmstadt).
[37] H.L. Tolman, D. Chalikov, Source terms in a third-generation wind wave model, J. Phys. Oceanogr. 26 (11) (1996) 2497–2518.
[38] S. Aijaz, W.E. Rogers, A.V. Babanin, Wave spectral response to sudden changes in wind direction in finite-depth waters, Ocean. Model. 103 (2016) 98–117.
[39] M.M. Amrutha, V.S. Kumar, K.G. Sandhya, T.M.B. Nair, J.L. Rathod, Wave hindcast studies using SWAN nested in WAVEWATCH III - comparison with measured nearshore buoy data off Karwar, eastern Arabian Sea, Ocean. Eng. 119 (2016) 114–124.
[40] S. Saha, S. Moorthi, H.L. Pan, X.R. Wu, J.D. Wang, S. Nadiga, P. Tripp, R. Kistler, J. Woollen, D. Behringer, H.X. Liu, D. Stokes, R. Grumbine, G. Gayno, J. Wang, Y.T. Hou, H.Y. Chuang, H.M.H. Juang, J. Sela, M. Iredell, R. Treadon, D. Kleist, P. Van Delst, D. Keyser, J. Derber, M. Ek, J. Meng, H.L. Wei, R.Q. Yang, S. Lord, H. Van den Dool, A. Kumar, W.Q. Wang, C. Long, M. Chelliah, Y. Xue, B.Y. Huang, J.K. Schemm, W. Ebisuzaki, R. Lin, P.P. Xie, M.Y. Chen, S.T. Zhou, W. Higgins, C.Z. Zou, Q.H. Liu, Y. Chen, Y. Han, L. Cucurull, R.W. Reynolds, G. Rutledge, M. Goldberg, The NCEP climate forecast system reanalysis, Bull. Am. Meteorological Soc. 91 (8) (2010) 1015–1057.
[41] S. Saha, S. Moorthi, X.R. Wu, J. Wang, S. Nadiga, P. Tripp, D. Behringer, Y.T. Hou, H.Y. Chuang, M. Iredell, M. Ek, J. Meng, R.Q. Yang, M.P. Mendez, H. Van Den Dool, Q. Zhang, W.Q. Wang, M.Y. Chen, E. Becker, The NCEP climate forecast system version 2, J. Clim. 27 (6) (2014) 2185–2208.
[42] L. Cavaleri, P.M. Rizzoli, Wind wave prediction in shallow-water - theory and applications, J. Geophys. Res. Oceans Atmos. 86 (Nc11) (1981) 961–973.
[43] P.A.E.M. Janssen, Wave-induced stress and the drag of air-flow over sea waves, J. Phys. Oceanogr. 19 (6) (1989) 745–754.
[44] P.A.E.M. Janssen, Quasi-linear theory of wind-wave generation applied to wave forecasting, J. Phys. Oceanogr. 21 (11) (1991) 1631–1642.
[45] J.A. Battjes, J.P.F.M. Janssen, Energy loss and set-up due to breaking random waves, in: 16th Conference on Coastal Engineering, ASCE, Hamburg, Germany, 1978.
[46] S. Hasselmann, K. Hasselmann, J.H. Allender, T.P. Barnett, Computations and parameterizations of the nonlinear energy-transfer in a gravity-wave spectrum .2. Parameterizations of the nonlinear energy-transfer for application in wave models, J. Phys. Oceanogr. 15 (11) (1985) 1378–1391.
[47] NDBC, Handbook of Automated Data Quality Control Checks and Procedures, NDBC Technical Document 09-02, 2009, p. 78.
[48] F. Bi, J.B. Song, K.J. Wu, Y. Xu, Evaluation of the simulation capability of the WAVEWATCH III model for Pacific Ocean wave, Acta Oceanol. Sin. 34 (9) (2015) 43–57.
[49] J.E. Stopa, K.F. Cheung, Intercomparison of wind and wave data from the ECMWF reanalysis interim and the NCEP climate forecast system reanalysis, Ocean. Model. 75 (2014) 65–83.
[50] C.R. Sampson, P.A. Wittmann, E.A. Serra, H.L. Tolman, J. Schauer, T. Marchok, Evaluation of wave forecasts consistent with tropical cyclone warning center wind forecasts, Weather Forecast. 28 (1) (2013) 287–294.

Please cite this article in press as: Z. Yang, et al., A wave model test bed study for wave energy resource characterization, Renewable Energy (2017), http://dx.doi.org/10.1016/j.renene.2016.12.057